

# Runnings in the Curvaton

Takeshi Kobayashi <sup>1,2,3</sup> and Tomo Takahashi <sup>4</sup>

<sup>1</sup>*Research Center for the Early Universe, School of Science, The University of Tokyo,  
7-3-1 Hongo, Bunkyo-ku, Tokyo 113-0033, Japan*

<sup>2</sup>*Canadian Institute for Theoretical Astrophysics, University of Toronto,  
60 St. George Street, Toronto, Ontario M5S 3H8, Canada*

<sup>3</sup>*Perimeter Institute for Theoretical Physics,  
31 Caroline St. N, Waterloo, Ontario N2L 2Y5, Canada*

<sup>4</sup>*Department of Physics, Saga University, Saga 840-8502, Japan*

We investigate the scale-dependence, or the runnings, of linear and second order density perturbations generated in various curvaton scenarios. We argue that the second order perturbations, i.e. non-Gaussianity, can strongly depend on the scale, even when the linear perturbations are nearly scale-invariant. We present analytic formulae for the runnings from curvatons with general energy potentials, and clarify the conditions under which  $f_{\text{NL}}$  becomes strongly scale-dependent. From the point of view of the  $f_{\text{NL}}$  running, curvaton potentials can be classified into roughly two categories by whether the potential flattens or steepens compared to a quadratic one. As such examples, we study pseudo-Nambu-Goldstone curvatons, and self-interacting curvatons, respectively. The dynamics of non-quadratic curvatons and the behaviors of the resulting density perturbations are clarified by analytical methods. Then we also study models where multiple source can be responsible for density perturbations such as the multi-curvaton, and mixed curvaton and inflaton models where the running of  $f_{\text{NL}}$  can also be large due to their multi-source nature. We make quantitative analysis for each curvaton scenario and discuss in what cases the scale-dependence, in particular, of  $f_{\text{NL}}$  can be large enough to be probed with future CMB experiments.

# Contents

<b>1</b>	<b>Introduction</b>	<b>1</b>
<b>2</b>	<b>Scale-Dependence of <math>f_{\text{NL}}</math> in the Curvaton Mechanism</b>	<b>3</b>
2.1	Density Perturbations . . . . .	3
2.2	Scale-Dependence . . . . .	7
<b>3</b>	<b>Pseudo-Nambu-Goldstone Curvatons</b>	<b>10</b>
<b>4</b>	<b>Self-Interacting Curvatons</b>	<b>15</b>
<b>5</b>	<b>Mixed Curvaton and Inflaton</b>	<b>23</b>
<b>6</b>	<b>Multi-curvaton</b>	<b>28</b>
6.1	Both curvaton subdominant at their decays . . . . .	30
6.2	Both curvaton dominant at their decays . . . . .	33
<b>7</b>	<b>Conclusions</b>	<b>35</b>
<b>A</b>	<b>Density Perturbations from Curvatons with Non-Sinusoidal Oscillations</b>	<b>36</b>

## 1 Introduction

The origin of density fluctuations in the Universe is one of the important issues in cosmology and also gives invaluable information for high energy physics since they are assumed to be generated in the very early Universe. Although quantum fluctuations of the inflaton, which drives inflation in the very early Universe, has been considered to be its origin over the years, other mechanisms have also been discussed. Among possible candidates, the curvaton scenario [1–3] has been attracting much attention due to several reasons, one of which is the recent observational results on primordial non-Gaussianity. How much the primordial fluctuations deviate from a Gaussian distribution can be characterized by the non-linearity parameter  $f_{\text{NL}}$ , whose constraint from current observations is  $-10 < f_{\text{NL}} < 74$  (95 % C.L.) [4] for the so-called local type non-Gaussianity<sup>#1</sup>. If future data such as those from the on-going Planck satellite confirms large local type non-Gaussianity of primordial fluctuations at the level of  $f_{\text{NL}} \gtrsim \mathcal{O}(10)$ , it readily excludes conventional single-field inflation models predicting  $f_{\text{NL}} \ll \mathcal{O}(1)$  as the origin of the density perturbations. On the other hand, the curvaton can generate large non-Gaussianity at this level, which would motivate us to seriously consider this scenario. Furthermore, the curvaton may be well fitted naturally into some particle physics

---

<sup>#1</sup>In this paper we mainly discuss local type non-Gaussianities. For constraints on  $f_{\text{NL}}$  of other types, see [4].

or string theory models (see, for e.g., [5–17]), thus also in this respect, the curvaton has been the target of intense study.

In many works on the curvaton model, it is assumed that the potential for the curvaton has a simple quadratic form and the curvaton is totally responsible for cosmic density fluctuations. However, such assumptions are removed in some microscopic constructions of the curvaton. Regarding the former assumption, there exist models realizing potentials that deviate from a purely quadratic one. The consequences of such non-quadratic curvaton potentials have been investigated for the self-interacting curvaton [18–24] and the pseudo-Nambu-Goldstone (NG) boson one [25–28]. Interestingly, it has been shown that the predictions for non-Gaussianity of the primordial perturbations significantly depend on the form of the potential. In particular, when the potential deviates from the quadratic form, the non-linearity parameter  $f_{\text{NL}}$  (and also other parameters characterizing non-Gaussianity such as  $\tau_{\text{NL}}$  and  $g_{\text{NL}}$  for the trispectrum) can be considerably scale-dependent [29–33], even when the linear order perturbations are nearly scale-invariant. On the other hand, the assumption of the curvaton being totally responsible for the density perturbations is removed for multi-source scenarios, where the scale dependence of non-Gaussianity can arise even with quadratic curvaton potentials [29,30]. Such a situation can be realized in the mixed curvaton and inflaton model [34–38] where fluctuations from the curvaton and inflaton can be both responsible for cosmic density perturbation today. One could also consider a model where there exist multiple curvaton fields and they can be responsible for density fluctuations. Some authors have studied a model of two curvatons [39,40].

It should also be noted that in the event of a detection of large non-Gaussianity, upcoming CMB experiments can set severe constraints on the scale-dependence of  $f_{\text{NL}}$  as well, especially when combined with large-scale structure surveys, see e.g. [41–44]. Such information beyond  $f_{\text{NL}}$  would be a powerful probe of the physics of the early universe. In the light of these considerations, the issue of the scale-dependence or “running” of non-Gaussianity is an interesting and important subject.

In this paper we carry out analytical studies of density perturbations from curvatons, by applying the method developed in [28]. We derive generic formulae for the runnings of the linear and second order density perturbations, which enable us to go beyond individual case studies and give a systematic treatment of the scale-dependence of  $f_{\text{NL}}$  in the curvaton mechanism. Our study not only serves as an analytical counterpart to previous works that basically relied on numerical computations, but also clarifies the underlying reason why strongly scale-dependent non-Gaussianities can be generated from non-quadratic curvatons. Furthermore, we present conditions for curvatons to produce large running of  $f_{\text{NL}}$ , which turn out to take simple forms (2.34) and (2.35) for a single curvaton. In passing, we also investigate the running of the spectral index of the power spectrum  $\alpha$ , which can also give interesting signatures. We will clarify the direct relation between  $\alpha$  and the running of  $f_{\text{NL}}$ , which we parametrize as  $n_{f_{\text{NL}}}$ . The general study of  $n_{f_{\text{NL}}}$  and  $\alpha$  would give new insight into the curvaton mechanism.

Curvaton potentials can roughly be categorized by whether they flatten or steepen compared to a quadratic one. It will be shown that this classification is important for discussing  $n_{f_{\text{NL}}}$  from curvatons. As typical examples of the two cases, we will look into pseudo-Nambu-Goldstone curvatons and self-interacting curvatons, respectively. For the former case, the relation between  $n_{f_{\text{NL}}}$  and  $\alpha$  plays an important role, restricting the running of  $f_{\text{NL}}$  from current observational bounds on  $\alpha$ . On the other hand, for the latter case, strongly scale-dependent  $f_{\text{NL}}$  can be produced even for a suppressed  $\alpha$  due to the steepness of the potential. Regarding  $n_{f_{\text{NL}}}$  generated in multi-source models, we make a quantitative study for some models and show in what cases the scale dependence can be large enough to be probed in future cosmological observations.

The structure of this paper is as follows: In Section 2 we derive analytic expressions for the scale-dependence of the linear and second order density perturbations from a curvaton. Then we move on and apply the generic discussions to pseudo-Nambu-Goldstone curvatons in Section 3, and self-interacting curvatons in Section 4. In Section 5, we further investigate the issue for the mixed curvaton and inflaton scenario. Then in Section 6, we discuss multi-curvaton model. We present our conclusions in Section 7.

We give a brief discussion on density perturbations from curvatons with non-sinusoidal oscillations in Appendix A.

## 2 Scale-Dependence of $f_{\text{NL}}$ in the Curvaton Mechanism

A light curvaton acquires nearly scale-invariant field fluctuations during inflation, that are converted into the cosmological density perturbations as the curvaton oscillates and decays in the post-inflationary era. In this section we derive generic expressions for the running of non-Gaussianity from a curvaton, and discuss the conditions under which the curvaton sources a largely scale-dependent  $f_{\text{NL}}$ . Our discussions in this section are based on the work [28] which developed analytic methods for computing density perturbations in the curvaton mechanism. We extend their results and compute the runnings of the linear and second order perturbations. In this Section and also in the following Sections 3 and 4, we assume that density perturbations sourced from the inflaton are neglected. However, we remove this assumption in Section 5 where we study the mixed curvaton and inflaton scenario.

### 2.1 Density Perturbations

Let us start by laying out some results of [28] for density perturbations produced by a curvaton  $\sigma$  possessing an effective potential  $V(\sigma)$ . The potential is assumed to have no explicit dependence on time, and also that it is well approximated by a quadratic one around its minimum so that the curvaton oscillations are sinusoidal<sup>#2</sup>. The curvaton energy density is

---

<sup>#2</sup>The formulae can be generalized to cases with non-sinusoidal oscillations as well, see Appendix B of [28].

considered to redshift similarly to nonrelativistic matter after the onset of the oscillations until when the curvaton decays into radiation, whereas we suppose the inflaton to behave as matter from the end of inflation until reheating (=inflaton decay), after which the inflaton turns into radiation. The energy density of the curvaton before the beginning of its oscillation is assumed to be negligibly tiny compared to the total energy of the Universe, having little effect on the expansion history. Furthermore, the Hubble parameter during inflation is considered to be nearly constant. For detailed discussions on the derivations of the following results, we refer the reader to [28].

Using the  $\delta\mathcal{N}$ -formalism [45–48], the density perturbations are obtained by computing quantities such as the time when the curvaton oscillation starts and the curvaton energy density as functions of the curvaton field value  $\sigma_*$  (hereafter the subscript  $*$  denotes values when the CMB scale  $k_*$  exits the horizon). The curvaton dynamics prior to the oscillation can be tracked by the attractor solution

$$\hat{c}H\dot{\sigma} = -V', \quad \text{with} \quad \hat{c} = \begin{cases} 3 & (\text{during inflation}) \\ 9/2 & (\text{matter domination}) \\ 5 & (\text{radiation domination}) \end{cases}, \quad (2.1)$$

which is a good approximation while  $|V''/\hat{c}H^2| \ll 1$ . Here, a prime denotes a derivative with respect to  $\sigma$ , and an overdot a time derivative. Setting the minimum of the potential about which the curvaton oscillates to  $\sigma = 0$ , we can define the onset of the oscillation as when the time scale of the curvaton rolling becomes comparable to the Hubble time, i.e.  $|\dot{\sigma}/H\sigma| = 1$ . This, combined with (2.1), gives the Hubble parameter at the time,

$$H_{\text{osc}}^2 = \frac{V'(\sigma_{\text{osc}})}{c\sigma_{\text{osc}}}, \quad (2.2)$$

where the subscript “osc” denotes values at the onset of the curvaton oscillation, and  $c$  is a constant whose value is set by whether reheating (= inflaton decay, at  $t_{\text{reh}}$ ) is earlier/later than the onset of the curvaton oscillation:

$$c = \begin{cases} 5 & (t_{\text{reh}} < t_{\text{osc}}) \\ 9/2 & (t_{\text{reh}} > t_{\text{osc}}). \end{cases} \quad (2.3)$$

We define the power spectrum  $\mathcal{P}_\zeta$  of the density perturbations  $\zeta$  as

$$\langle \zeta_{\mathbf{k}} \zeta_{\mathbf{k}'} \rangle = (2\pi)^3 \delta^{(3)}(\mathbf{k} + \mathbf{k}') P_\zeta(k) \quad \text{with} \quad P_\zeta(k) = \frac{2\pi^2}{k^3} \mathcal{P}_\zeta(k), \quad (2.4)$$

where  $k \equiv |\mathbf{k}|$ . Supposing the curvaton field fluctuations to satisfy  $\mathcal{P}_{\delta\sigma}(k) = (H|_{k=aH}/2\pi)^2$  at the time when the scale  $k$  exits the horizon, then the linear order density perturbations at the CMB scale can be expressed in terms of the curvaton potential as

$$\mathcal{P}_\zeta(k_*) = \left( \frac{\partial \mathcal{N}}{\partial \sigma_*} \frac{H_*}{2\pi} \right)^2, \quad (2.5)$$

with

$$\frac{\partial \mathcal{N}}{\partial \sigma_*} = \frac{\hat{r}}{4 + 3\hat{r}} (1 - X(\sigma_{\text{osc}}))^{-1} \left\{ \frac{V'(\sigma_{\text{osc}})}{V(\sigma_{\text{osc}})} - \frac{3X(\sigma_{\text{osc}})}{\sigma_{\text{osc}}} \right\} \frac{V'(\sigma_{\text{osc}})}{V'(\sigma_*)}. \quad (2.6)$$

Here,  $\hat{r}$  is the energy density ratio between the curvaton and radiation (which originates from the inflaton) upon curvaton decay<sup>#3</sup>

$$\hat{r} \equiv \left. \frac{\rho_\sigma}{\rho_r} \right|_{\text{dec}}, \quad (2.8)$$

while the function  $X$  denotes effects due to the non-uniform onset of the curvaton oscillations (which are absent for a purely quadratic curvaton potential), defined as follows:

$$X(\sigma_{\text{osc}}) \equiv \frac{1}{2(c-3)} \left( \frac{\sigma_{\text{osc}} V''(\sigma_{\text{osc}})}{V'(\sigma_{\text{osc}})} - 1 \right). \quad (2.9)$$

From the bispectrum

$$\langle \zeta_{\mathbf{k}_1} \zeta_{\mathbf{k}_2} \zeta_{\mathbf{k}_3} \rangle = (2\pi)^3 \delta^{(3)}(\mathbf{k}_1 + \mathbf{k}_2 + \mathbf{k}_3) B_\zeta(k_1, k_2, k_3), \quad (2.10)$$

one can generally define the non-linearity parameter  $f_{\text{NL}}$  as

$$B_\zeta(k_1, k_2, k_3) = \frac{6}{5} f_{\text{NL}}(k_1, k_2, k_3) [P_\zeta(k_1)P_\zeta(k_2) + P_\zeta(k_2)P_\zeta(k_3) + P_\zeta(k_3)P_\zeta(k_1)]. \quad (2.11)$$

However, upon parameterizing the overall amplitude of the local-type bispectra produced by curvatons,<sup>#4</sup> throughout this paper we discuss  $f_{\text{NL}}$  on the equilateral configuration

$$f_{\text{NL}}(k) \equiv \frac{5}{18} B_\zeta(k, k, k) \left( \frac{2\pi^2}{k^3} \mathcal{P}_\zeta(k) \right)^{-2}. \quad (2.13)$$

We suppose that the bispectrum of the curvaton fluctuations  $\langle \delta\sigma_{\mathbf{k}_1} \delta\sigma_{\mathbf{k}_2} \delta\sigma_{\mathbf{k}_3} \rangle$  with  $|\mathbf{k}_1|=|\mathbf{k}_2|=|\mathbf{k}_3|=k$  vanishes when  $k$  exits the horizon, and further neglect direct trispectra of  $\delta\sigma$  (i.e.  $\langle \delta\sigma_{\mathbf{q}_1} \delta\sigma_{\mathbf{q}_2} \delta\sigma_{\mathbf{q}_3} \delta\sigma_{\mathbf{q}_4} \rangle = \langle \delta\sigma_{\mathbf{q}_1} \delta\sigma_{\mathbf{q}_2} \rangle \langle \delta\sigma_{\mathbf{q}_3} \delta\sigma_{\mathbf{q}_4} \rangle + (2 \text{ perm.})$ ). Then it can be shown that  $f_{\text{NL}}$

---

<sup>#3</sup>The following quantity is also used in the literature to express the formulae for density perturbations from the curvaton:

$$r_{\text{dec}} = \left. \frac{3\rho_\sigma}{4\rho_r + 3\rho_\sigma} \right|_{\text{dec}}, \quad (2.7)$$

which is also evaluated at the curvaton decay. Notice that  $\hat{r}$  defined here is a bit different from  $r_{\text{dec}}$ .

<sup>#4</sup>It should also be noted that, especially when  $f_{\text{NL}}$  is strongly scale-dependent, the bispectrum (2.10) sourced from a curvaton has shapes similar to, but not exactly of the “local form” [49] which is often given as

$$B_{\text{local}}(k_1, k_2, k_3) \propto \frac{1}{k_1^3 k_2^3} + \frac{1}{k_1^3 k_3^3} + \frac{1}{k_2^3 k_3^3}. \quad (2.12)$$

takes the form [28],

$$\begin{aligned}
f_{\text{NL}}(k_*) &= \frac{5}{6} \frac{\partial^2 \mathcal{N}}{\partial \sigma_*^2} \left( \frac{\partial \mathcal{N}}{\partial \sigma_*} \right)^{-2} \\
&= \frac{40(1+\hat{r})}{3\hat{r}(4+3\hat{r})} + \frac{5(4+3\hat{r})}{6\hat{r}} \left\{ \frac{V'(\sigma_{\text{osc}})}{V(\sigma_{\text{osc}})} - \frac{3X(\sigma_{\text{osc}})}{\sigma_{\text{osc}}} \right\}^{-1} \left[ (1-X(\sigma_{\text{osc}}))^{-1} X'(\sigma_{\text{osc}}) \right. \\
&\quad + \left\{ \frac{V'(\sigma_{\text{osc}})}{V(\sigma_{\text{osc}})} - \frac{3X(\sigma_{\text{osc}})}{\sigma_{\text{osc}}} \right\}^{-1} \left\{ \frac{V''(\sigma_{\text{osc}})}{V(\sigma_{\text{osc}})} - \frac{V'(\sigma_{\text{osc}})^2}{V(\sigma_{\text{osc}})^2} - \frac{3X'(\sigma_{\text{osc}})}{\sigma_{\text{osc}}} + \frac{3X(\sigma_{\text{osc}})}{\sigma_{\text{osc}}^2} \right\} \\
&\quad \left. + \frac{V''(\sigma_{\text{osc}})}{V'(\sigma_{\text{osc}})} - (1-X(\sigma_{\text{osc}})) \frac{V''(\sigma_*)}{V'(\sigma_{\text{osc}})} \right]. \tag{2.14}
\end{aligned}$$

The scale-dependence of  $f_{\text{NL}}$  shows up through  $\sigma_*$ , whereas  $\sigma_{\text{osc}}$  and  $\hat{r}$  are independent of the wave number. Hence for later convenience, let us divide the expression into terms that explicitly depend on  $\sigma_*$ , and the rest,

$$f_{\text{NL}} = f_1(\sigma_*, \sigma_{\text{osc}}, \hat{r}) + f_2(\sigma_{\text{osc}}, \hat{r}), \tag{2.15}$$

where we have introduced

$$\begin{aligned}
f_1 &\equiv -\frac{5(4+3\hat{r})}{6\hat{r}} \left\{ \frac{V'(\sigma_{\text{osc}})}{V(\sigma_{\text{osc}})} - \frac{3X(\sigma_{\text{osc}})}{\sigma_{\text{osc}}} \right\}^{-1} (1-X(\sigma_{\text{osc}})) \frac{V''(\sigma_*)}{V'(\sigma_{\text{osc}})} \\
&= -\frac{5}{6} \left( \frac{\partial \mathcal{N}}{\partial \sigma_*} \right)^{-1} \frac{V''(\sigma_*)}{V'(\sigma_*)}. \tag{2.16}
\end{aligned}$$

Upon obtaining the second line, we have used (2.6)<sup>#5</sup>.

---

<sup>#5</sup>For a curvaton with a quadratic potential  $V \propto \sigma^2$ , one obtains

$$\frac{\partial \mathcal{N}}{\partial \sigma_*} = \frac{2\hat{r}}{4+3\hat{r}} \frac{1}{\sigma_*}, \quad \frac{\partial^2 \mathcal{N}}{\partial \sigma_*^2} = \frac{2\hat{r}(16+8\hat{r}-9\hat{r}^2)}{(4+3\hat{r})^3} \frac{1}{\sigma_*^2}. \tag{2.17}$$

Furthermore, the terms  $f_1$  and  $f_2$  depend only on  $\hat{r}$ ,

$$f_1 = -\frac{5(4+3\hat{r})}{12\hat{r}}, \quad f_2 = \frac{40(1+\hat{r})}{3\hat{r}(4+3\hat{r})}, \tag{2.18}$$

and thus

$$f_{\text{NL}} = \frac{5}{12} \left( -3 + \frac{4}{\hat{r}} + \frac{8}{4+3\hat{r}} \right). \tag{2.19}$$

Large non-Gaussianity is generated for  $\hat{r} \ll 1$ , under which

$$f_{\text{NL}} \simeq -f_1 \simeq \frac{1}{2} f_2 \simeq \frac{5}{3\hat{r}}. \tag{2.20}$$

The energy density ratio  $\hat{r}$  (2.8) is obtained as

$$\hat{r} = \text{Max.} \left[ \frac{V(\sigma_{\text{osc}})}{3M_p^2 H_{\text{osc}}^{3/2} \Gamma_\sigma^{1/2}} \times \text{Min.} \left( 1, \frac{\Gamma_\phi^{1/2}}{H_{\text{osc}}^{1/2}} \right), \right. \\ \left. \left\{ \frac{V(\sigma_{\text{osc}})}{3M_p^2 H_{\text{osc}}^{3/2} \Gamma_\sigma^{1/2}} \times \text{Min.} \left( 1, \frac{\Gamma_\phi^{1/2}}{H_{\text{osc}}^{1/2}} \right) \right\}^{4/3} \right], \quad (2.21)$$

where the first and second terms in the Max. parentheses correspond to the curvaton being subdominant and dominant at its decay, respectively, while the Min. parentheses are due to whether the onset of oscillation is after or before reheating.  $\Gamma_\phi$  and  $\Gamma_\sigma$  are constants denoting respectively the decay rates of the inflaton and the curvaton. Throughout we adopt the sudden decay approximation where the scalar fields suddenly decay into radiation when  $H = \Gamma$ .

The curvaton field value at the onset of the oscillations  $\sigma_{\text{osc}}$  is obtained by integrating (2.1),

$$\int_{\sigma_*}^{\sigma_{\text{osc}}} \frac{d\sigma}{V'} = -\frac{\mathcal{N}_*}{3H_{\text{inf}}^2} - \frac{1}{2c(c-3)H_{\text{osc}}^2}, \quad (2.22)$$

solving which gives  $\sigma_{\text{osc}}$  as a function of  $\sigma_*$ <sup>#6</sup>. Here,  $\mathcal{N}_*$  is the number of e-folds during inflation between the horizon exit of the CMB scale and the end of inflation, and  $H_{\text{inf}}$  is the inflationary Hubble scale (we are assuming a nearly constant Hubble parameter during inflation, thus  $H_{\text{inf}} \simeq H_*$ ). Let us also show the derivative of  $\sigma_{\text{osc}}$ ,

$$\frac{\partial \sigma_{\text{osc}}}{\partial \sigma_*} = (1 - X(\sigma_{\text{osc}}))^{-1} \frac{V'(\sigma_{\text{osc}})}{V'(\sigma_*)}, \quad (2.23)$$

which has entered (2.6) through  $\partial \mathcal{N} / \partial \sigma_* \propto \partial \sigma_{\text{osc}} / \partial \sigma_*$ .

Thus by combining the above expressions, one can compute the resulting density perturbations from a curvaton with a generic potential  $V(\sigma)$ , given the curvaton field value at the CMB scale horizon exit  $\sigma_*$ , the decay rates of the inflaton  $\Gamma_\phi$  and curvaton  $\Gamma_\sigma$ , the inflationary scale  $H_{\text{inf}}$ , and the duration of inflation  $\mathcal{N}_*$ .

## 2.2 Scale-Dependence

Now we extend the above expressions to discuss the scale-dependence of the linear and second order density perturbations, which are the main topic of this paper.

Since we are assuming  $|\dot{H}/H^2| \ll 1$  during inflation, the comoving wave number  $k$  at around the CMB scale satisfies

$$d \ln k \simeq H_* dt. \quad (2.24)$$

---

<sup>#6</sup>When (2.22) admits as solutions for  $\sigma_{\text{osc}}$  both positive and negative values, one should take the sign of  $\sigma_{\text{osc}}$  to match with that of  $\sigma_*$ .



Then by using the slow-roll approximation for the curvaton

$$3H_*\dot{\sigma}_* \simeq -V'(\sigma_*), \quad (2.25)$$

one obtains the spectral index of the linear order perturbations at the CMB scale

$$n_s - 1 \equiv \frac{d}{d \ln k} \ln \mathcal{P}_\zeta \simeq 2 \frac{\dot{H}_*}{H_*^2} + \frac{2}{3} \frac{V''(\sigma_*)}{H_*^2}, \quad (2.26)$$

as well as its running

$$\alpha \equiv \frac{dn_s}{d \ln k} \simeq 2 \frac{\ddot{H}_*}{H_*^3} - 4 \frac{\dot{H}_*^2}{H_*^4} - \frac{4}{3} \frac{\dot{H}_*}{H_*^2} \frac{V''(\sigma_*)}{H_*^2} - \frac{2}{9} \frac{V'(\sigma_*)V'''(\sigma_*)}{H_*^4}. \quad (2.27)$$

Focusing on the contributions to the scale-dependence that are sourced purely by the tilt of the curvaton potential, we introduce the following parameters

$$\tilde{n}_s - 1 \equiv \frac{2}{3} \frac{V''(\sigma_*)}{H_*^2}, \quad (2.28)$$

$$\tilde{\alpha} \equiv -\frac{2}{9} \frac{V'(\sigma_*)V'''(\sigma_*)}{H_*^4}. \quad (2.29)$$

When the Hubble parameter during inflation is exactly a constant, these give the spectral index and its running at the leading order, i.e.  $n_s \simeq \tilde{n}_s$  and  $\alpha \simeq \tilde{\alpha}$ .

In order to parametrize the scale-dependence of the non-Gaussianity, we define the spectral index of  $f_{\text{NL}}$  as follows:

$$n_{f_{\text{NL}}} \equiv \frac{d \ln |f_{\text{NL}}|}{d \ln k}. \quad (2.30)$$

We remark that a totally scale-invariant  $f_{\text{NL}}$  corresponds to  $n_{f_{\text{NL}}} = 0$  (instead of 1). Then, in a similar fashion as above, one arrives at

$$n_{f_{\text{NL}}} \simeq \frac{1}{f_{\text{NL}}} \frac{5(4 + 3\hat{r})}{18\hat{r}} \left\{ \frac{V'(\sigma_{\text{osc}})}{V(\sigma_{\text{osc}})} - \frac{3X(\sigma_{\text{osc}})}{\sigma_{\text{osc}}} \right\}^{-1} (1 - X(\sigma_{\text{osc}})) \frac{V'(\sigma_*)}{V'(\sigma_{\text{osc}})} \frac{V'''(\sigma_*)}{H_*^2}. \quad (2.31)$$

Here we note that time derivatives of  $H_*$  do not show up at the leading order, since  $f_{\text{NL}}$  (2.14) does not explicitly depend on the Hubble parameter during inflation. One clearly sees that a non-vanishing  $n_{f_{\text{NL}}}$  (at the leading order) requires non-zero  $V'''(\sigma_*)$ , and hence  $f_{\text{NL}}$  produced by a curvaton with a quadratic potential is scale-invariant. This opens up the possibility that a slight deviation of the curvaton potential from a quadratic one can be verified through observing the running of  $f_{\text{NL}}$ .

By using (2.6), one can simplify (2.31) as

$$n_{f_{\text{NL}}} \simeq \frac{1}{f_{\text{NL}}} \frac{5}{18} \left( \frac{\partial \mathcal{N}}{\partial \sigma_*} \right)^{-1} \frac{V'''(\sigma_*)}{H_*^2}, \quad (2.32)$$

which shows that when the power spectrum is fixed to a certain value, e.g. from the COBE (WMAP) normalization, then the value of the product  $n_{f_{\text{NL}}} f_{\text{NL}}$  is determined only by information at the CMB scale horizon exit.

Moreover, in terms of the parameters (2.16), (2.28), and (2.29), the expression (2.31) can be recast into the form of

$$n_{f_{\text{NL}}} \simeq \frac{\tilde{\alpha}}{\tilde{n}_s - 1} \frac{f_1}{f_{\text{NL}}}. \quad (2.33)$$

This equation makes clear the typical amplitude of the running of  $f_{\text{NL}}$  expected in the curvaton model. In simple cases, the running parameter  $\tilde{\alpha}$  (though not necessarily equivalent to the actual running of the spectral index) has a smaller size than the spectral index parameter  $\tilde{n}_s - 1$ . Furthermore, since  $f_1$  explicitly depends on  $\sigma_*$  while the rest of the terms of  $f_{\text{NL}}$  do not<sup>#7</sup>, one may not expect  $f_1$  to be much larger than the sum  $f_{\text{NL}} = f_1 + f_2$ . Thus naively one would expect the running of  $f_{\text{NL}}$  from curvatons to be highly suppressed.

In other words,  $n_{f_{\text{NL}}}$  as large as, say  $|n_{f_{\text{NL}}}| \gtrsim 1$ , is realized only when at least one of the following two conditions are satisfied:

$$|\tilde{\alpha}| \gtrsim |\tilde{n}_s - 1|, \quad (2.34)$$

$$|f_1| \gtrsim |f_{\text{NL}}|. \quad (2.35)$$

The former condition (2.34) may be realized by curvaton potentials possessing inflection points, or more generally, by potentials that flatten compared to a quadratic as one goes away from the minimum. As such an example, in Section 3 we study pseudo-Nambu-Goldstone curvatons with cosine-type potentials. However, there we will see that the resulting  $n_{f_{\text{NL}}}$  is actually directly bounded by observational constraints on the running  $\alpha$  of the spectral index of the linear order perturbations. The latter condition (2.35) indicates that  $f_1$  and  $f_2$  cancel each other, suppressing  $f_{\text{NL}}$  compared to  $f_1$ . Such suppression of  $f_{\text{NL}}$  is known to exist for self-interacting curvatons possessing polynomial terms that are higher order than quadratic, as was numerically shown in [18–24]. In Section 4 we look into self-interacting curvatons and see that large  $n_{f_{\text{NL}}}$  can be obtained even under a suppressed running  $\alpha$ , and further discuss that such behavior stems from the curvaton potential steepening more rapidly than quadratic ones.

The value of  $f_{\text{NL}}$  itself needs to be large for its running to be detectable, and thus experiments are sensitive to the product  $n_{f_{\text{NL}}} f_{\text{NL}}$ , instead of  $n_{f_{\text{NL}}}$  alone. Upon discussing example models in the following sections, we refer to the results of [42] where detectability of a scale-dependent non-Gaussianity through CMB experiments are analyzed<sup>#8</sup>. The running of the

---

<sup>#7</sup>Strictly speaking,  $\sigma_{\text{osc}}$  also depends on  $\sigma_*$  through (2.22), but the point here is that  $f_1$  and  $f_2$  depend quite differently on  $\sigma_*$ .

<sup>#8</sup>We note that the definition of our running parameter  $n_{f_{\text{NL}}}$  (2.30) is not exactly the same as the  $n_{\text{NG}}$  parameter adopted in [42], especially in the sense that  $n_{\text{NG}}$  is set to a constant whereas  $n_{f_{\text{NL}}}$  itself can run. Nevertheless we adopt their results upon discussing detectability.

local-type  $f_{\text{NL}}$  can be probed if it is large enough to satisfy

$$|n_{f_{\text{NL}}}| > A \times \frac{50}{f_{\text{NL}}}, \quad (2.36)$$

where the right hand side takes  $A \simeq 0.68$ ,  $0.10$ , and  $0.05$  for WMAP [4], Planck [50], and CMBPol [51], respectively, assuming as fiducial values  $f_{\text{NL}} = 50$ ,  $n_{f_{\text{NL}}} = 0$ , and a full-sky coverage.

Before ending this section, we should mention about errors in the analytic formulae. Firstly, the approximation (2.24) contains error of order  $\dot{H}_*/H_*^2$ , and (2.25) of order  $V''(\sigma_*)/H_*^2$ . By taking into account such errors, one can check that they do not modify the above results on  $n_s$ ,  $\alpha$ , and  $n_{f_{\text{NL}}}$  at the leading order.

However further approximations and simplifications have been carried out upon obtaining the analytic expressions of Subsection 2.1, e.g., the approximation (2.1) on the curvaton dynamics, which is correct up to order  $V''/H^2$ . This can source errors in the results of order  $V''/H^2$ , and also of derivatives of  $V''/H^2$  in terms of  $\sigma_*$  and/or time  $t$ . It should be noted that such error with various orders of derivatives can accumulate and lead to breakdown of the analytic expressions especially for higher-order correlation functions and running. Nevertheless, for the explicit examples we study in the following sections, we will see that the analytic results match well with results from numerical computations.

### 3 Pseudo-Nambu-Goldstone Curvatons

Since the parameters  $\tilde{n}_s$  and  $\tilde{\alpha}$  in the expression for  $n_{f_{\text{NL}}}$  (2.33) are not necessarily the actual spectral index and its running under a non-vanishing  $\dot{H}$  during inflation, one may expect that the condition (2.34) for a large  $n_{f_{\text{NL}}}$  is easily satisfied without contradicting with observational constraints on the flatness of the power spectrum. One may imagine cases where the amplitudes of  $\tilde{\alpha}$  and  $\tilde{n}_s - 1$  are much smaller than unity, though possessing a hierarchy among them as  $|\tilde{\alpha}| \gg |\tilde{n}_s - 1|$ .

In this section we study the case where the curvaton is realized as a pseudo-Nambu-Goldstone (NG) boson of a broken U(1) symmetry, possessing a cosine-type potential [25–28]. Given that the curvaton at the CMB scale horizon exit is located close to the inflection point of the potential,  $\tilde{n}_s - 1$  vanishes while  $\tilde{\alpha}$  remains finite. However, we will see that the resulting  $n_{f_{\text{NL}}}$  is actually set by the absolute value of  $\tilde{\alpha}$ , thus bounded by observational constraints on the running of the spectral index (unless  $\tilde{\alpha}$  is cancelled out by the  $\dot{H}$  terms in (2.27)).

We consider the potential of the form

$$V(\sigma) = \Lambda^4 \left[ 1 - \cos \left( \frac{\sigma}{f} \right) \right], \quad (3.1)$$

where  $f$  and  $\Lambda$  are mass scales. It has inflection points at  $\sigma/f = (1/2 + n)\pi$  with  $n \in \mathbf{Z}$ , and we focus on the region  $0 < \sigma_{\text{osc}}/f, \sigma_*/f < \pi$  without loss of generality. Since

$$\tilde{n}_s - 1 = \frac{2}{3} \frac{\Lambda^4}{H_*^2 f^2} \cos\left(\frac{\sigma_*}{f}\right), \quad (3.2)$$

$$\tilde{\alpha} = \frac{2}{9} \frac{\Lambda^8}{H_*^4 f^4} \sin^2\left(\frac{\sigma_*}{f}\right), \quad (3.3)$$

one sees that  $\tilde{\alpha}/(\tilde{n}_s - 1)$  blows up at  $\sigma_*/f = \pi/2$ . However,  $n_{\text{fNL}}$  is actually set by the value itself of  $\tilde{\alpha}$  as we will soon see.

In Figures 2 - 7, we display the density perturbations plotted as a function of  $\sigma_*/f$  under the parameter set  $\Lambda = 10^{15}$  GeV and  $f = 10^{17}$  GeV, along with the inflationary parameters  $H_{\text{inf}} = 3.5 \times 10^{13}$  GeV,  $\Gamma_\phi = 10^{11}$  GeV (i.e. the energy density at reheating (= inflaton decay) is  $\rho_{\text{reh}}^{1/4} \approx 6.5 \times 10^{14}$  GeV), and  $\mathcal{N}_* = 50$ .<sup>#9</sup> The curvaton decay rate is set to  $\Gamma_\sigma = \frac{1}{16\pi} \frac{V''(0)^{3/2}}{f^2} = \frac{1}{16\pi} \frac{\Lambda^6}{f^5}$ , supposing that the coupling of the NG curvaton with its decay product is suppressed by the symmetry breaking scale  $f$ . This set of parameters are chosen such that the COBE (WMAP) normalization value [4]  $\mathcal{P}_\zeta \approx 2.4 \times 10^{-9}$  as well as  $\tilde{n}_s \approx 0.96$  are realized at around  $\sigma_*/\pi f \approx 0.8$ .<sup>#10</sup> Moreover, the curvaton starts its oscillation before reheating, thus  $c = 9/2$ .

$\sigma_{\text{osc}}$  is computed by solving (2.22), which now takes the form

$$\ln \left[ \frac{\tan(\sigma_{\text{osc}}/2f)}{\tan(\sigma_*/2f)} \right] = -\frac{\mathcal{N}_*}{3H_{\text{inf}}^2} \frac{\Lambda^4}{f^2} - \frac{1}{2(c-3)} \frac{\sigma_{\text{osc}}/f}{\sin(\sigma_{\text{osc}}/f)}. \quad (3.4)$$

By obtaining a fitting function for the solution  $\sigma_{\text{osc}}(\sigma_*)$  (which is shown in Figure 1), we have analytically calculated the density perturbations in terms of  $\sigma_*$ . The analytically estimated results are shown as blue solid lines in Figures 2 - 7 for the region  $0.01 \lesssim \sigma_*/\pi f \lesssim 0.99$ .

We have also numerically computed the density perturbations, by solving the curvaton's equation of motion and computing the differences in the number of e-foldings obtained from different initial values  $\sigma_*$ . Upon carrying out the numerical computations, we have set the inflaton energy to a constant during inflation which lasts for 50 e-foldings after the CMB scale exits the horizon, then transferred the inflaton energy to non-relativistic matter redshifting as  $\rho \propto a^{-3}$ , and finally to radiation as  $\rho \propto a^{-4}$ . Furthermore, we adopted the sudden decay approximation for the inflaton/curvaton, as well as a sudden end of inflation. The numerically

---

<sup>#9</sup>The e-folding number  $\mathcal{N}_*$  is basically determined by knowing the scale of inflation and the subsequent expansion history. However in order to clarify the dependence of the density perturbations on each parameter, we fix  $\mathcal{N}_*$  to 50 in Sections 3 and 4. The direct consequence of a larger (smaller)  $\mathcal{N}_*$  is to decrease (increase)  $\sigma_{\text{osc}}$ , hence does not affect  $n_s$  nor  $\alpha$ , while other cosmological observables can be affected, especially since  $\hat{r}$  is also changed. Nevertheless, the overall behavior of the density perturbations are not influenced much by the detailed value of  $\mathcal{N}_*$ . Thus the fixing of  $\mathcal{N}_*$  does not affect our discussions greatly.

<sup>#10</sup>The inflationary scale needs to be rather high when one tries to realize the COBE (WMAP) normalization and  $|\tilde{n}_s - 1| \sim 0.01$  at  $\sigma_*$  values not so close to the hilltop [28]. For such high-scale inflation, depending on the inflationary mechanism, density perturbations from the inflaton can also become substantial.

computed results are shown as blue dots in the figures. Since we have fixed the inflaton energy density to a constant during inflation, the spectral index (2.26) and its running (2.27) are expected to match with the parameters  $\tilde{n}_s$  (2.28) and  $\tilde{\alpha}$  (2.29), respectively, at the leading order. Thus we have displayed  $\tilde{n}_s$  and  $\tilde{\alpha}$ , and the numerically computed  $n_s$  and  $\alpha$  in the same plots in Figures 2 and 3. One sees that the analytic estimations are in good agreement with the results of the numerical calculations in all Figures 2 - 7.

In most of the displayed  $\sigma_*/f$  region the behavior of the density perturbations from a NG curvaton can be understood similarly as for a curvaton with a quadratic potential (cf. Footnote #5), except for around the hilltop  $\sigma_* \approx \pi f$  where the linear perturbations and  $f_{\text{NL}}$  are enhanced. (In the figures we have plotted up to  $\sigma_*/\pi f \lesssim 0.99$ , however as one goes even closer to the hilltop,  $\mathcal{P}_\zeta$  and  $f_{\text{NL}}$  further increase, cf. [28].)

The amplitude of the running of the non-Gaussianity  $n_{f_{\text{NL}}}$  is more or less correlated with the  $\tilde{\alpha}$  parameter, which is independent of the energy fraction  $\hat{r}$ . This is a rather generic feature of density perturbations from a NG curvaton, which can be understood from (2.32),

$$n_{f_{\text{NL}}} \simeq -\frac{5}{18} \frac{1}{f_{\text{NL}}} \left( \frac{\partial \mathcal{N}}{\partial \sigma_*} \right)^{-1} \frac{\Lambda^4}{H_*^2 f^3} \sin \left( \frac{\sigma_*}{f} \right) = \left( -\frac{6}{5} f_{\text{NL}} \cdot \frac{\partial \mathcal{N}}{\partial \sigma_*} \cdot \sigma_* \right)^{-1} \frac{\sigma_*}{f} \sqrt{\frac{\tilde{\alpha}}{2}}. \quad (3.5)$$

In the far right hand side, the product inside the parentheses is a combination whose amplitude is smaller than unity for quadratic curvatons.<sup>#11</sup> Here, recall that the density perturbations from a NG curvaton are more or less the same as those from a quadratic curvaton, except for the hilltop region. Therefore the  $()^{-1}$  term in the far right hand side of (3.5) is roughly of order unity (except for when  $f_{\text{NL}}$  vanishes), and accordingly,  $|n_{f_{\text{NL}}}|$  is roughly of order  $\sqrt{\tilde{\alpha}}$ . On the other hand, when  $|f_{\text{NL}}| \ll 1$ , the product inside the parentheses also becomes much smaller than unity and thus its inverse blows up (though not seen in Figure 6, this can happen depending of the parameter set). However, in such a case the product  $n_{f_{\text{NL}}} f_{\text{NL}}$  to which experiments are sensitive is suppressed. Hence one can conclude that the running of  $f_{\text{NL}}$  from a NG curvaton is basically set by the absolute value of  $\tilde{\alpha}$ , which is constrained by current observational bounds on a running spectral index<sup>#12</sup> (unless the time-variation of the Hubble parameter cancels out  $\tilde{\alpha}$  from (2.27)).

As mentioned above, the produced perturbations behave quite differently as one approaches the hilltop, i.e.  $\sigma_*/f \rightarrow \pi$ . However there the potential is well approximated by a quadratic, i.e.  $V \simeq V_0 - m^2 \sigma^2$ , hence  $\tilde{\alpha}$  approaches zero and  $n_{f_{\text{NL}}}$  is suppressed.

We show contours in the  $n_{f_{\text{NL}}} - f_{\text{NL}}$  planes from a NG curvaton in Figures 8 and 9. Instead of choosing a certain parameter set for e.g.  $\Lambda$  and  $f$  as in the previous figures, here we have

---

<sup>#11</sup>A quadratic curvaton  $V \propto \sigma^2$  gives

$$-\frac{6}{5} f_{\text{NL}} \cdot \frac{\partial \mathcal{N}}{\partial \sigma_*} \cdot \sigma_* = \frac{9\hat{r}^2 - 8\hat{r} - 16}{(3\hat{r} + 4)^2}, \quad (3.6)$$

which monotonically increases with  $\hat{r}$ , and approaches  $+(-)1$  in the limit  $\hat{r} \gg (\ll)1$ .

<sup>#12</sup>The current observational  $1\sigma$  limit for the running spectral index from WMAP7 is  $\alpha = -0.034 \pm 0.026$  [4].

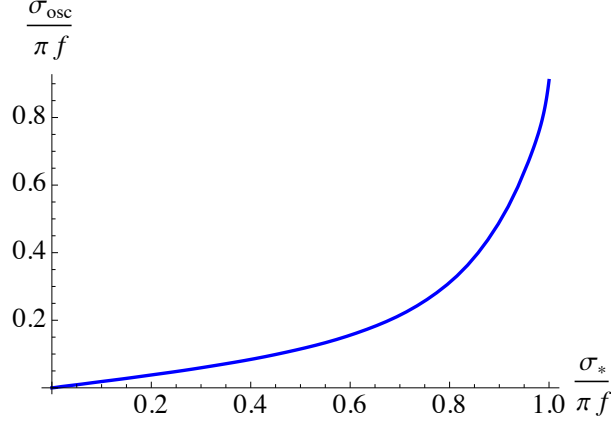


Figure 1:  $\sigma_{\text{osc}}$  as a function of  $\sigma_*$ .

fixed  $\tilde{n}_s$  to 0.96 and 1.04, respectively, and plotted the contours in the following way: For a given  $\tilde{n}_s$ , by using (3.2) one can rewrite  $\Lambda^4/H_{\text{inf}}^2 f^2$  in terms of  $\sigma_*/f$ . Hence  $f_{\text{NL}}$  as well as  $n_{f_{\text{NL}}}$  are uniquely determined by  $\sigma_*/f$ ,  $\sigma_{\text{osc}}/f$ ,  $\hat{r}$ ,  $\tilde{n}_s$ , and  $c$ . Furthermore,  $\sigma_{\text{osc}}/f$  is given as a function of  $\sigma_*/f$  after solving (3.4) (note that  $\Lambda^4/H_{\text{inf}}^2 f^2$  is now determined by  $\tilde{n}_s$  and  $\sigma_*/f$ ), where we took  $\mathcal{N}_* = 50$  and  $c = 9/2$ , i.e.  $t_{\text{reh}} > t_{\text{osc}}$  (taking instead  $c = 5$ , i.e.  $t_{\text{reh}} < t_{\text{osc}}$ , makes little difference for the resulting contours). Each colored solid line in the figures is plotted for a fixed value of  $\sigma_*/\pi f$ , under a varying  $\hat{r}$ . Different values for  $\sigma_*/\pi f$  give different values for  $\tilde{\alpha}$ : blue, green, and red lines correspond to  $\tilde{\alpha} \approx 0.05$ , 0.008, and  $8 \times 10^{-5}$ , respectively. We note that this procedure for plotting the contours does not fix the linear perturbation amplitude, i.e., the individual values for  $\Lambda$ ,  $f$ , and  $H_{\text{inf}}$  can be varied to change the perturbation amplitude for a fixed  $\Lambda^4/H_{\text{inf}}^2 f^2$ . As reference values for detectability, we have also shown  $n_{f_{\text{NL}}} f_{\text{NL}}/50 = 0.10$  contours as black dashed lines. Outside these contours corresponds to the region detectable by Planck, cf. (2.36).

Taking smaller  $\hat{r}$  ( $\ll 1$ ) corresponds to moving upwards along the colored contour lines. It is clearly seen that a large  $n_{f_{\text{NL}}} f_{\text{NL}}$  is realized for larger values of  $\tilde{\alpha}$ , as was discussed below (3.5). Since the contours in the two figures are chosen to take the same values for  $\tilde{\alpha}$ , they are more or less the same in the  $\hat{r} \ll 1$  regime.

On the other hand, as  $\hat{r}$  is increased, the contour lines eventually turn left and  $n_{f_{\text{NL}}}$  decreases. There the blue contours realize  $|n_{f_{\text{NL}}}|$  much larger than  $|\alpha|$ , due to the suppressed  $|f_{\text{NL}}| \ll 1$ . In some cases  $f_{\text{NL}}$  can even cross zero (as it happens for quadratic curvatures, cf. (3.6)), which is accompanied by  $n_{f_{\text{NL}}}$  blowing up and changing sign. This is seen in Figure 9 as the contour lines extending towards  $n_{f_{\text{NL}}} \rightarrow -\infty$ , and then coming back from the right. Although such behavior is absent in Figure 8, it can happen for  $\sigma_*/f > \pi/2$  cases as well, depending on the parameter values. Since the blowing up of  $n_{f_{\text{NL}}}$  happens when  $f_{\text{NL}}$  is tiny, its observational detection would be challenging, even if it happened. In the  $\hat{r} \rightarrow \infty$

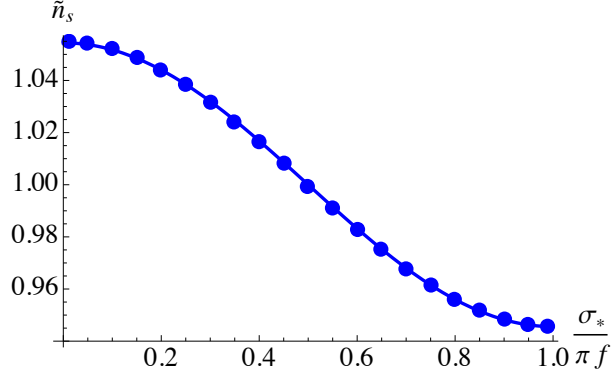


Figure 2: Curvaton contribution to the spectral index (2.28).

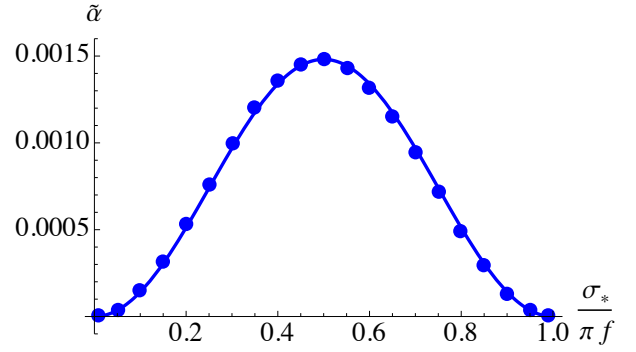


Figure 3: Curvaton contribution to the running of the spectral index (2.29).

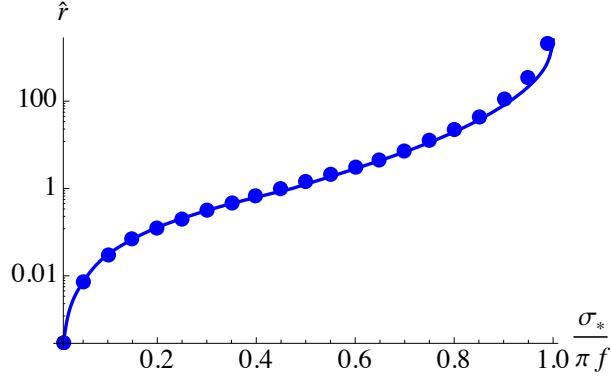


Figure 4: Energy fraction at decay.

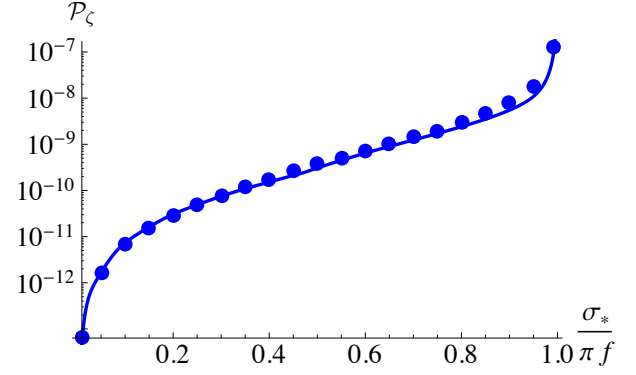


Figure 5: Linear order perturbations.

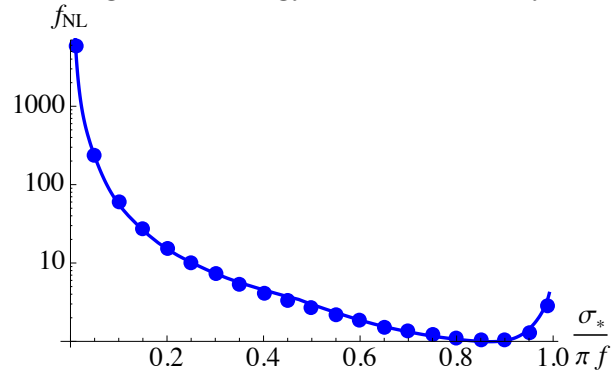


Figure 6: Non-Gaussianity.

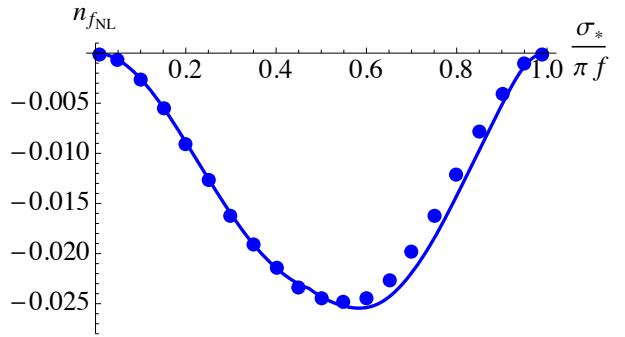


Figure 7: Running of non-Gaussianity.

limit,  $n_{f_{\text{NL}}}$  approaches a certain value, which can be seen as the end points of the contour lines. (The end points of the blue lines in both figures are outside the displayed region.)

Focusing on a contour line with a fixed value for  $\sigma_*/\pi f$ , then taking a larger value for  $|\tilde{n}_s - 1|$  is equivalent to increasing  $\tilde{\alpha}$ , hence the contour would shift towards larger  $|n_{f_{\text{NL}}}|$ . In summary, for NG curvaton, large  $|n_{f_{\text{NL}}} f_{\text{NL}}|$  is produced together with a large  $\tilde{\alpha}$ , therefore it is already strictly constrained by current observational bounds on running spectral index, unless  $\tilde{\alpha}$  is cancelled out from the expression for  $\alpha$  due to a varying Hubble parameter during inflation.

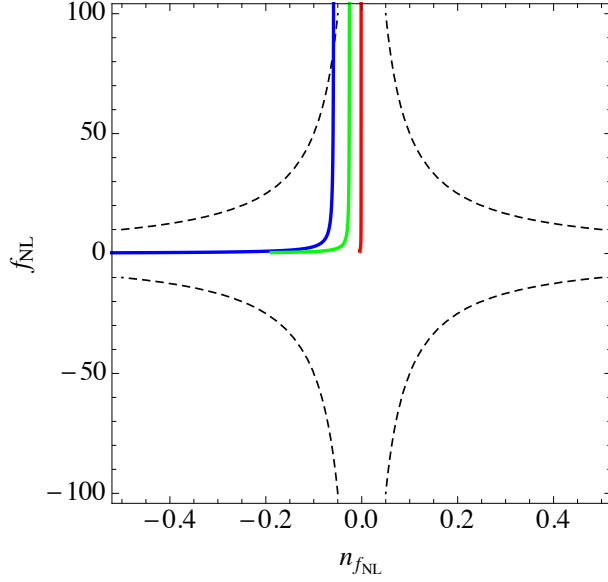


Figure 8: Varying  $\hat{r}$  under  $\tilde{n}_s = 0.96$ .  $\sigma_*/\pi f$  is fixed to 0.55 (blue), 0.60 (green), and 0.90 (red), corresponding to  $\tilde{\alpha} \approx 0.03$ , 0.008, and  $8 \times 10^{-5}$ , respectively. The expected observational sensitivity of Planck is also shown (black dashed).

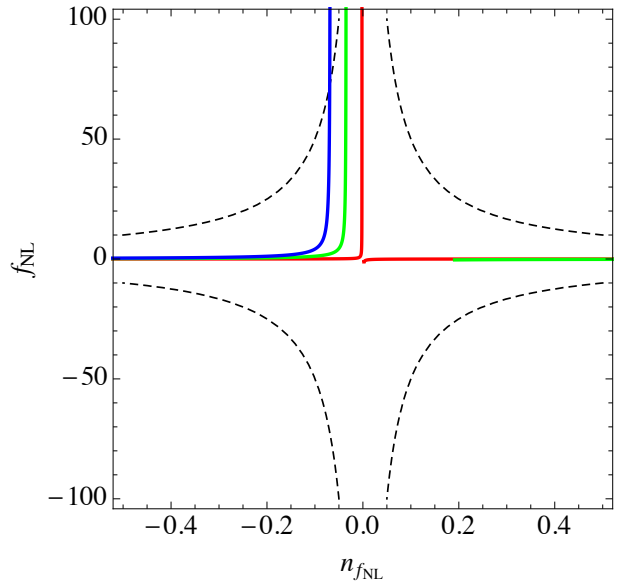


Figure 9: Varying  $\hat{r}$  under  $\tilde{n}_s = 1.04$ .  $\sigma_*/\pi f$  is fixed to 0.45 (blue), 0.40 (green), and 0.10 (red), corresponding to  $\tilde{\alpha} \approx 0.03$ , 0.008, and  $8 \times 10^{-5}$ , respectively.

## 4 Self-Interacting Curvatons

As a simple example of curvaton potentials that steepen more rapidly than a quadratic, in this section we explore curvatons possessing a mass term and an additional higher-order polynomial term [18–24]:

$$V(\sigma) = \Lambda^4 \left[ \left( \frac{\sigma}{f} \right)^2 + \left( \frac{\sigma}{f} \right)^m \right], \quad (4.1)$$



where  $\Lambda$  and  $f$  are positive constants with mass dimension, and  $m$  is an even integer with  $m > 2$ .  $f$  denotes where the higher-order term becomes important, while  $\Lambda$  sets the overall scale of the curvaton potential. Furthermore, the curvaton mass at the potential minimum is given by  $M_\sigma^2 = 2\Lambda^4/f^2$ . We especially focus on the region  $|\sigma| \lesssim f$ , where the analytic expressions give good estimations of the resulting curvature perturbations and a large running of  $f_{\text{NL}}$  can show up. The validity of the analytic expressions at large  $\sigma$  values are discussed towards the end of this section.

The potential (4.1) gives

$$\tilde{n}_s - 1 = \frac{4}{3} \frac{\Lambda^4}{H_*^2 f^2} \left\{ 1 + \frac{m(m-1)}{2} \left( \frac{\sigma_*}{f} \right)^{m-2} \right\}, \quad (4.2)$$

$$\tilde{\alpha} = -\frac{4m(m-1)(m-2)}{9} \frac{\Lambda^8}{H_*^4 f^4} \left( \frac{\sigma_*}{f} \right)^{m-2} \left\{ 1 + \frac{m}{2} \left( \frac{\sigma_*}{f} \right)^{m-2} \right\}, \quad (4.3)$$

where one can see that the resulting  $n_s$  and  $\alpha$  are positive and negative, respectively, for  $\sigma_* \neq 0$ . We also note that  $-\frac{\tilde{\alpha}}{(\tilde{n}_s-1)^2}$  takes its maximum value  $\frac{m-1}{8}$  at  $(\frac{\sigma_*}{f})^{m-2} = \frac{2}{m(m-3)}$ . Hence especially for  $m \lesssim 10$ , then  $-\tilde{\alpha} \lesssim (\tilde{n}_s - 1)^2$ .

Let us now examine  $\sigma_{\text{osc}}$  since understanding its behavior in terms of  $\sigma_*$  is essential for discussing largely scale-dependent  $f_{\text{NL}}$  produced from self-interacting curvatons. The Hubble parameter at the onset of oscillation (2.2) is

$$H_{\text{osc}}^2 = \frac{1}{c} \frac{\Lambda^4}{f^2} \left( 2 + m \left( \frac{\sigma_{\text{osc}}}{f} \right)^{m-2} \right), \quad (4.4)$$

thus the relation (2.22) between  $\sigma_*$  and  $\sigma_{\text{osc}}$  becomes

$$\ln \left[ \frac{m + 2(\sigma_*/f)^{-(m-2)}}{m + 2(\sigma_{\text{osc}}/f)^{-(m-2)}} \right] = -(m-2) \left\{ \frac{2}{3} \mathcal{N}_* \frac{\Lambda^4}{H_{\text{inf}}^2 f^2} + \frac{1}{c-3} \left( 2 + m \left( \frac{\sigma_{\text{osc}}}{f} \right)^{m-2} \right)^{-1} \right\}. \quad (4.5)$$

By solving this equation,  $\sigma_{\text{osc}}$  is obtained as a function of  $\sigma_*$ . (Here  $\sigma_{\text{osc}}$  should take the same sign as  $\sigma_*$ , cf. Footnote #6.) We do this numerically, as shown in Figure 11, but the behavior of  $\sigma_{\text{osc}}$  can simply be understood by rewriting (4.5) as<sup>#13</sup>

$$2 \left( \frac{\sigma_*}{f} \right)^{-(m-2)} = -m + \left( m + 2 \left( \frac{\sigma_{\text{osc}}}{f} \right)^{-(m-2)} \right) \times \exp \left[ -(m-2) \left\{ \frac{2}{3} \mathcal{N}_* \frac{\Lambda^4}{H_{\text{inf}}^2 f^2} + \frac{1}{c-3} \left( 2 + m \left( \frac{\sigma_{\text{osc}}}{f} \right)^{m-2} \right)^{-1} \right\} \right]. \quad (4.6)$$

---

<sup>#13</sup>Here we exponentiate both sides of the equation in order to make clear the behavior of its solution, but let us note that since (2.22) itself is an approximate relation, one should in general be careful about the size of the errors when exponentiating the equation.

Since the left hand side of this equation is positive,  $\sigma_{\text{osc}}$  should not take values that make the right hand side negative, which can happen for e.g., large  $m$ ,  $|\sigma_{\text{osc}}/f|$ , and  $\mathcal{N}_*\Lambda^4/H_{\text{inf}}^2f^2$ . Such values of  $\sigma_{\text{osc}}$  are displayed in Figure 10, where regions of the  $\sigma_{\text{osc}}/f$  -  $m$  plane on the right sides of the lines give negative values to the right hand side of (4.6). For example, when  $m = 8$  and  $\mathcal{N}_*\Lambda^4/H_{\text{inf}}^2f^2 = 1$ , then  $\sigma_{\text{osc}} \gtrsim 0.3f$  cannot be a solution of (4.6), i.e. the curvaton rolls down before it starts its oscillations to values smaller than about  $0.3f$  even if  $\sigma$  during inflation takes much larger field values<sup>#14</sup>. Such behavior is in contrast to a quadratic curvaton, for which one can check that  $\sigma_{\text{osc}} \propto \sigma_*$ . In Figure 11 we plot  $\sigma_{\text{osc}}$  as a function of  $\sigma_*$  by numerically solving (4.5) for  $m = 8$  and  $\mathcal{N}_*\Lambda^4/H_{\text{inf}}^2f^2 = 1$ . One sees that the growing rate of  $\sigma_{\text{osc}}$  is suppressed at  $\sigma_* \sim f$  where the curvaton potential steepens due to the higher-order self-interaction, and that  $\sigma_{\text{osc}}$  is limited to values smaller than  $\sim 0.3f$  as is indicated in Figure 10. Such flattening of  $\sigma_{\text{osc}}$  is more significant for larger values of  $m$  and  $\Lambda^4/H_{\text{inf}}^2f^2$  which make the potential steeper, and for larger  $\mathcal{N}_*$  providing a longer period for the curvaton to roll down during inflation.

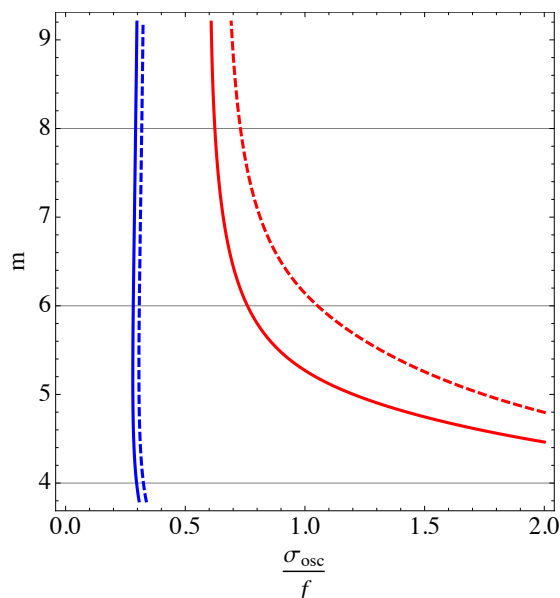


Figure 10: The right hand side of (4.6) becomes negative on the right sides of the lines. Blue and red lines denote  $\mathcal{N}_*\Lambda^4/H_{\text{inf}}^2f^2 = 1$  and  $10^{-2}$ , while solid and dashed lines denote  $c = 9/2$  and  $5$ , respectively.

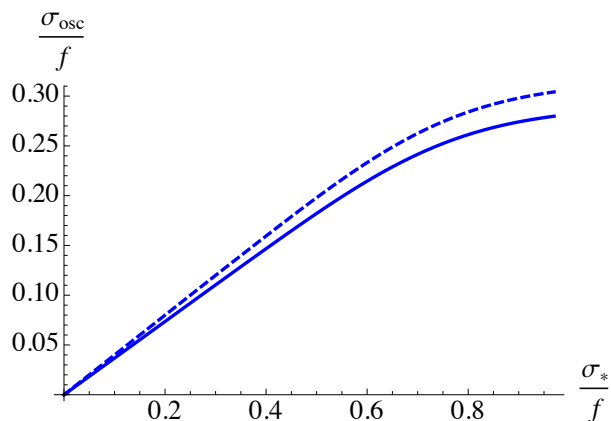


Figure 11:  $\sigma_{\text{osc}}$  as a function of  $\sigma_*$ , for  $m = 8$  and  $\mathcal{N}_*\Lambda^4/H_{\text{inf}}^2f^2 = 1$ . Solid and dashed lines denote  $c = 9/2$  and  $5$ , respectively.

The rolling of the curvaton due to the steep potential makes  $\sigma_{\text{osc}}$  substantially smaller

<sup>#14</sup>Of course, discussions here are basically limited to curvaton field values that satisfy the approximation (2.1) until the onset of the oscillations.

than  $\sigma_*$ , and as we will soon see, this leads to a running non-Gaussianity. Let us now show the density perturbations generated by a self-interacting curvaton with the parameter set  $m = 8$ ,  $\Lambda = 2.5 \times 10^{12}$  GeV,  $f = 4.3 \times 10^{13}$  GeV, and  $\Gamma_\sigma = 10^{-15}$  GeV (i.e. the energy density of the universe at the curvaton decay is  $\rho_{\text{dec}}^{1/4} \approx 65$  GeV), along with the inflationary parameters  $H_{\text{inf}} = 10^{12}$  GeV,  $\Gamma_\phi = 3.8 \times 10^3$  GeV (i.e. the energy density at reheating (= inflaton decay) is  $\rho_{\text{reh}}^{1/4} \approx 1.3 \times 10^{11}$  GeV), and  $\mathcal{N}_* = 50$  (see also Footnote #9). This set of parameters gives  $\Lambda^4/H_{\text{inf}}^2 f^2 \approx 0.02$  (which determines the magnitude of  $\tilde{n}_s - 1$ ), and realizes the COBE (WMAP) normalization value as well as  $\hat{r} \sim 10^{-2}$  at around  $\sigma_*/f \approx 0.6$ , where  $n_{f_{\text{NL}}}$  blows up. The curvaton starts its oscillation before reheating, thus  $c = 9/2$ . The value of  $\sigma_{\text{osc}}$  in terms of  $\sigma_*$  for this parameter set is illustrated by the blue solid line in Figure 11. Along with the analytic calculations, we also carried out numerical computations for the density perturbations in a similar fashion as we have done for NG curvatons in Section 3. The results are shown as functions of  $\sigma_*/f$  in Figures 12 - 18, where the blue solid lines denote the analytic calculations and the blue dots the numerically computed results. Upon the numerical computations we have fixed the inflaton energy density to a constant during inflation, thus plotted  $\tilde{n}_s$  and  $\tilde{\alpha}$ , and the numerically computed  $n_s$  and  $\alpha$  in the same figures. In the presence of nonzero  $\dot{H}_*$  or  $\ddot{H}_*$ , the actual spectral index and its running obtain offsets as shown in (2.26) and (2.27). For example, a  $\phi^6$  type chaotic inflation with  $\mathcal{N}_* = 50$  realizes  $n_s = \tilde{n}_s - 0.06$ <sup>#15</sup>, and thus red-tilts the resulting perturbation spectrum at  $\sigma_*/f \approx 0.6$  where  $n_{f_{\text{NL}}}$  blows up.

We also note that for the above parameter set, the curvaton's classical rolling in a Hubble time is larger than its quantum fluctuations during inflation, i.e.  $V'/3H_{\text{inf}}^2 > H_{\text{inf}}/2\pi$ , at around  $\sigma_*/f \approx 0.6$  and larger. Although this is not necessarily the case for smaller  $\sigma_*$  (for  $\sigma_*/f \lesssim 0.54$  the quantum fluctuations become dominant over the classical rolling by the end of inflation), we have plotted in the figures down to small  $\sigma_*$  regions supposing that the curvaton dynamics during inflation can be treated as classical, in order to see the full (classical)  $\sigma_*$ -dependence of the density perturbations<sup>#16</sup>.

The  $\sigma_* \ll f$  region is well-approximated by the familiar quadratic curvaton, but as one goes towards larger  $\sigma_*$ , the system starts to behave quite differently. The power spectrum of the linear order perturbations (2.5) in Figure 15 increases in the small field regime with  $\sigma_*$  due to the increase of  $\hat{r}$ . However for larger field values, the power spectrum starts to decrease as a function of  $\sigma_*$ . This is attributed to the behavior of  $\sigma_{\text{osc}}$  shown in Figure 11: When  $\sigma_*/f$  approaches unity,  $\sigma_{\text{osc}}$  ceases to grow as rapidly as  $\sigma_*$ , hence the terms in the expression (2.6) are insensitive to the value of  $\sigma_*$ , except through the explicit dependence

<sup>#15</sup> Although the  $\phi^6$  chaotic inflation model is excluded due to too large tensor-to-scalar ratio and red-tilted spectral index when the inflaton is totally responsible for the primordial density perturbation, in the curvaton framework, chaotic inflation models with high order polynomials are still viable.

<sup>#16</sup> We also remark that for the example parameters we have adopted, the classical rolling is not so large compared to the quantum fluctuations at around  $\sigma_*/f \approx 0.6$ , hence random effects from quantum fluctuations may also need to be taken into account for a more rigorous treatment.

$\partial\mathcal{N}/\partial\sigma_* \propto \partial\sigma_{\text{osc}}/\partial\sigma_* \propto 1/V'(\sigma_*)$ . As a consequence, the power spectrum becomes a decreasing function of  $\sigma_*$  for large field regime. In other words, in the large  $\sigma_*$  regime the steep potential forces the curvaton to roll down to take similar values for  $\sigma_{\text{osc}}$  almost independently of  $\sigma_*$ , therefore  $\partial\mathcal{N}_*/\partial\sigma_*$  is suppressed. The peak of the power spectrum is located in the intermediate region, i.e. at  $\sigma_* \approx 0.6f$ , and this roughly matches with the asymptotic value of  $\sigma_{\text{osc}}$  that can be read off from Figure 11 (or 10). When starting from large  $\sigma_*$ , the initial field fluctuations are reduced as the curvaton rolls down to field values below the asymptotic value of  $\sigma_{\text{osc}}$ , and thus the linear perturbations are suppressed.

The existence of the peak in the power spectrum indicates that the non-linearity parameter  $f_{\text{NL}}$  crosses zero and its running  $n_{f_{\text{NL}}}$  blows up. This is understood also in terms of  $f_1$  and  $f_2$  (2.15), which are plotted in addition to  $f_{\text{NL}}$  in Figure 16. At  $\sigma_* \ll f$  the amplitudes of  $f_1$  and  $f_2$  are comparable and their sum results in a positive  $f_{\text{NL}}$  as is the case for quadratic curvatons (cf. Footnote #5). However as one takes larger  $\sigma_*$ ,  $f_2$  which is a function of  $\sigma_{\text{osc}}$  and  $\hat{r}$  becomes insensitive to  $\sigma_*$ , while  $f_1$  rapidly decreases on the negative side through its explicit dependence on  $\sigma_*$ , resulting in a negative  $f_{\text{NL}}$ . One clearly sees that the condition (2.35) is satisfied at around  $\sigma_*/f \approx 0.6$  where  $f_{\text{NL}}$  crosses zero, being able to produce a large  $n_{f_{\text{NL}}}$  even under a suppressed  $\tilde{\alpha}$ . Furthermore, since  $\hat{r} \ll 1$ , the amplitude of  $f_{\text{NL}}$  itself is large (except for the very vicinity of its vanishing point) while satisfying (2.35), i.e.  $1 \ll |f_{\text{NL}}| \ll |f_1|$ . (This is in contrast to quadratic or NG curvatons, for which  $f_{\text{NL}}$  vanishes at rather large  $\hat{r}$ . This was why the product  $n_{f_{\text{NL}}} f_{\text{NL}}$  from NG curvatons was suppressed even when  $n_{f_{\text{NL}}}$  blew up, cf. Figure 9.) Therefore a large and strongly scale-dependent  $f_{\text{NL}}$  can be produced, whose running is in the detectable range by upcoming CMB observations. Contour lines in the  $n_{f_{\text{NL}}} - f_{\text{NL}}$  plane are shown in Figure 18, where the black dashed line denotes the Planck detection limit  $n_{f_{\text{NL}}} f_{\text{NL}}/50 = 0.10$ , cf. (2.36). Compared to the Figures 12 - 17, in Figure 18 we have added more numerically computed points, which are equally spaced in terms of  $\Delta\sigma_*$ .

Let us also comment on the validity of the analytic estimations. In most of the displayed region, the results from the analytic calculations are in good agreement with those from the numerical computations. However, as one goes towards larger  $\sigma_*$ , i.e. larger  $\sigma_{\text{osc}}$ , a period of non-sinusoidal oscillations along the  $\sigma^m$  potential needs to be taken into account. Thus the deviations between the analytic and numerical results which one can already see in, e.g. Figure 16, becomes even larger for  $\sigma_*$  beyond the region displayed in the figures. In Appendix A we extend the expressions in Section 2 to incorporate a period of non-sinusoidal oscillations, which becomes important for large  $\sigma_{\text{osc}}$  values. We also note that, with the choice of the parameter set here, the curvaton's effective mass during inflation is comparable to  $H_{\text{inf}}$  for  $\sigma_* \sim f$ , which violates the slow-roll approximation and sources additional errors to the analytic estimations.

For self-interacting curvatons with even larger  $\sigma_{\text{osc}}$ , we should remark that our approximations for the analytic expressions can break down. This is because, especially for cases with large  $m$  and  $\sigma_{\text{osc}}/f$ , the potential curvature  $V''$  quickly decreases after oscillation starts

(which we have defined by when  $|\dot{\sigma}/H\sigma| = 1$ ) as the curvaton rolls down to smaller field values. This forces the curvaton to recover (though not completely) the attractor dynamics (2.1) for a short time after  $t_{\text{osc}}$ . As a consequence, the simple picture of the curvaton suddenly starting its oscillations at  $t = t_{\text{osc}}$  is no longer a good approximation. Such breakdown of the approximations happen especially for large  $m$  or  $\sigma_*/f$ , or small  $\Lambda^4/H_{\text{inf}}^2 f^2$ , which realize large values for  $\sigma_{\text{osc}}$ . We also note that large  $m$  and  $\sigma_*$  can lead to the breakdown of the attractor solution (2.1) well before the onset of the oscillations, which can also spoil the analytic estimations. Density perturbations from a self-interacting curvaton with large  $\sigma_*$  values have been worked out numerically in [33].

In Figures 19 and 20 we further show contours in the  $n_{f_{\text{NL}}} - f_{\text{NL}}$  planes for a varying  $\sigma_*$  under fixed values of  $m$ ,  $\Lambda^4/H_{\text{inf}}^2 f^2$ , and  $\hat{r}$  (instead of fixing individual parameters). We have taken  $\mathcal{N}_* = 50$  and  $t_{\text{osc}} < t_{\text{reh}}$ , i.e.  $c = 9/2$ , but we remark that the results do not change significantly for  $t_{\text{osc}} > t_{\text{reh}}$ , i.e.  $c = 5$ . (It should also be noted that in order to compute  $f_{\text{NL}}$  and  $n_{f_{\text{NL}}}$ , we only need to specify  $m$ ,  $\Lambda^4/H_{\text{inf}}^2 f^2$ ,  $\hat{r}$ ,  $\sigma_*/f$ ,  $\mathcal{N}_*$ , and  $c$ . Note also that in order to determine the linear perturbation amplitude  $\mathcal{P}_\zeta$ , we further need to fix the ratio  $\Lambda/f$ .) Here we are fixing  $\hat{r}$ , which can be considered as varying  $\Gamma_\sigma$  along with  $\sigma_*/f$ , hence the resulting  $f_{\text{NL}}$  and  $n_{f_{\text{NL}}}$  can behave somewhat differently compared to Figures 16 - 18, especially in the region  $|\sigma_*| \ll f$ .

Steeper potentials, i.e., larger  $\Lambda^4/H_{\text{inf}}^2 f^2$  (or larger  $m$ ), realize flatter functions of  $\sigma_{\text{osc}}$  in terms of  $\sigma_*$ , which tend to produce  $f_{\text{NL}}$  with stronger scale-dependence as shown in Figure 19. Moreover, smaller  $\hat{r}$  basically leads to larger  $|f_{\text{NL}}|$ , pushing  $n_{f_{\text{NL}}}$  towards the detectable regions as one sees in Figure 20. A somewhat different behavior is seen for the  $\hat{r} \gg 1$  case shown as the red contour line in Figure 20, where  $f_{\text{NL}}$  is always negative and the  $\sigma_* \rightarrow 0$  limit corresponds to the endpoint of the line at  $n_{f_{\text{NL}}} = 0$ . This is understood as the  $\hat{r} \gg 1$  behavior of quadratic curvatons, cf. (2.19). Moreover, we have plotted the red line up to  $\sigma_*/f \approx 0.9$ , beyond which  $\tilde{n}_s$  becomes larger than 1.5 and the curvaton no longer slow-rolls during inflation. This corresponds to the other endpoint of the red line, where rather large  $|n_{f_{\text{NL}}}|$  (together with a largely negative  $f_{\text{NL}}$ ) is realized due the large  $\tilde{n}_s - 1$  and  $|\tilde{\alpha}|$ , coming close to satisfy the condition (2.34).

In summary, the steep potential forces the self-interacting curvaton to roll down to small field values by the onset of the curvaton oscillation. This greatly diminishes the initial differences in the curvaton field values during inflation  $\sigma_*$ , thus suppresses the resulting linear order density perturbations. When fixing all the parameters of the system except for  $\sigma_*$ , then a maximally large linear perturbation amplitude is obtained from  $\sigma_*$  that is close to the asymptotic value of  $\sigma_{\text{osc}}$ , and around this  $\sigma_*$  value is where a strongly scale-dependent  $f_{\text{NL}}$  is produced. We expect such behavior of a self-interacting curvaton to be a rather generic feature of curvatons whose potentials are approximated by quadratic around their minimum, but steepens more rapidly than a quadratic away from the minimum.

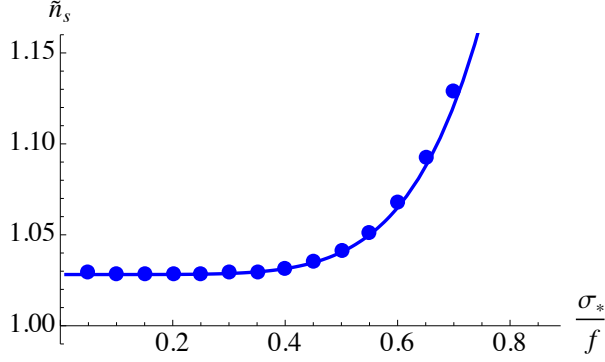


Figure 12: Curvaton contribution to the spectral index (2.28).

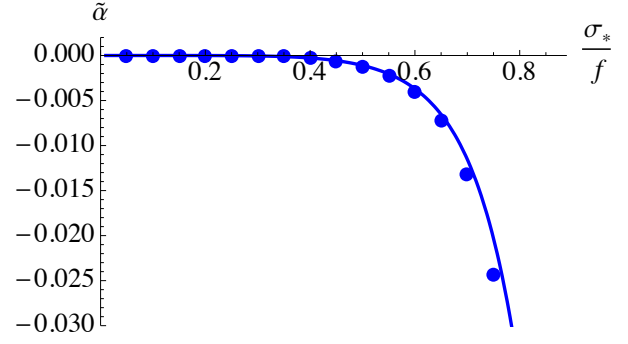


Figure 13: Curvaton contribution to the running of the spectral index (2.29).

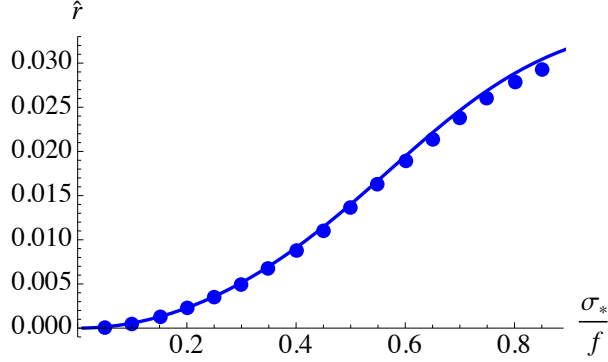


Figure 14: Energy fraction at decay.

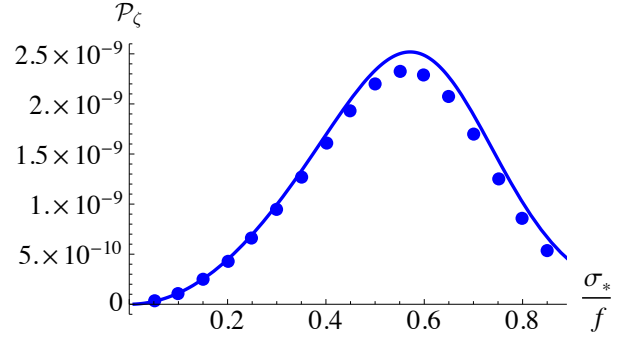


Figure 15: Linear order perturbations.

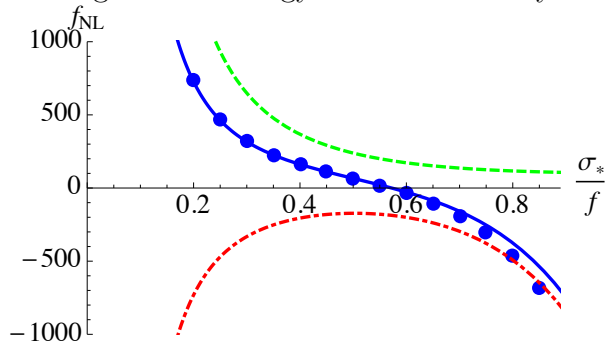


Figure 16: Non-Gaussianity.  $f_{\text{NL}}$ : blue solid,  $f_1$ : red dot-dashed,  $f_2$ : green dashed.

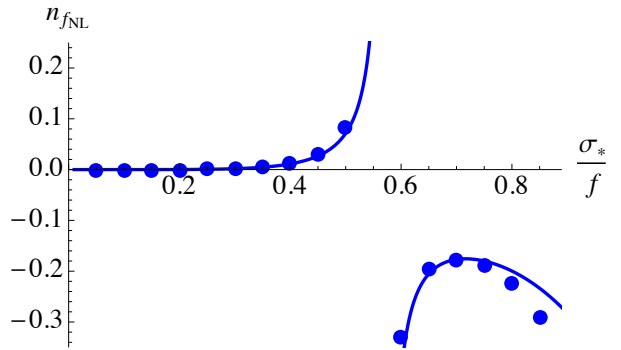


Figure 17: Running of non-Gaussianity.

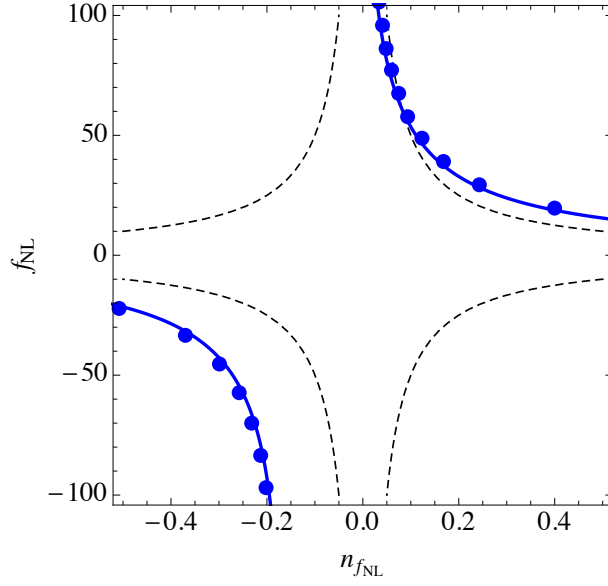


Figure 18: Plot in the  $n_{f_{\text{NL}}} - f_{\text{NL}}$  plane. The region  $0.45 \lesssim \sigma_*/f \lesssim 0.65$  is shown in the displayed area. The expected observational sensitivity of Planck is also shown (black dashed).

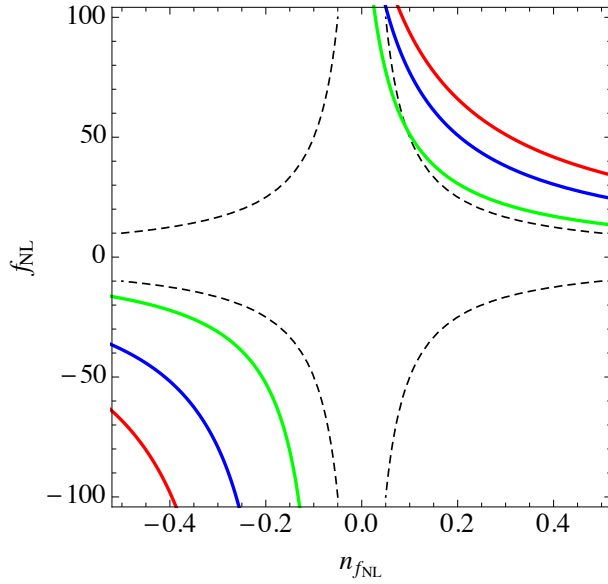


Figure 19: Varying  $\sigma_*/f$  for  $\Lambda^4/H_{\text{inf}}^2 f^2 = 0.03$  (red),  $0.02$  (blue),  $0.01$  (green), with fixed  $m = 8$  and  $\hat{r} = 10^{-2}$ . The expected observational sensitivity of Planck is also shown (black dashed).

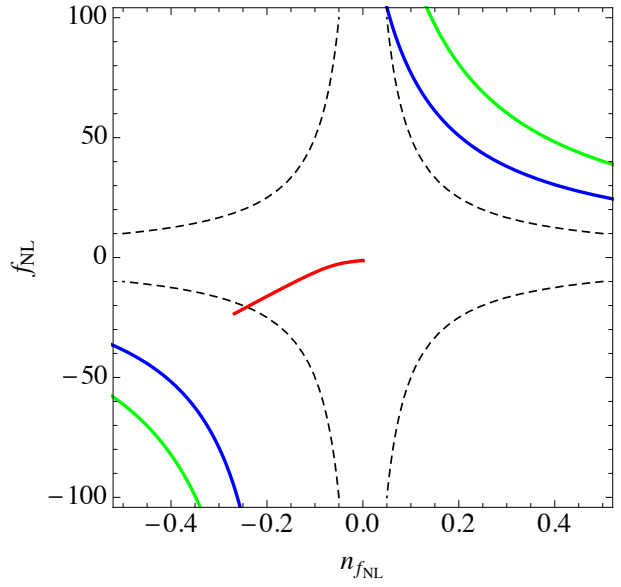


Figure 20: Varying  $\sigma_*/f$  for  $\hat{r} = 10^3$  (red),  $10^{-2}$  (blue),  $10^{-2.2}$  (green), with fixed  $m = 8$  and  $\Lambda^4/H_{\text{inf}}^2 f^2 = 0.02$ .

## 5 Mixed Curvaton and Inflaton

In the preceding two sections, we have assumed that fluctuations from the inflaton are negligible and those from the curvaton are only responsible for cosmic density fluctuations. But now in this section, we further consider the case where the inflaton  $\phi$  also contributes to the density perturbations as well as those from the curvaton, which is called “mixed curvaton and inflaton model” in the literature [34–38].

We start with giving the expression of the curvature perturbations in terms of the  $\delta\mathcal{N}$ -formalism, assuming that the field fluctuations of the inflaton  $\delta\phi$  and the curvaton  $\delta\sigma$  obey Gaussian distributions (to be more precise, in the sense discussed below (2.13)), with  $\mathcal{P}_{\delta\phi}(k) = \mathcal{P}_{\delta\sigma}(k) = (H|_{k=aH}/2\pi)^2$  when  $k$  exits the horizon. We further suppose that there are no direct couplings between the curvaton and inflation, thus no correlations between their fluctuations  $\delta\phi$  and  $\delta\sigma$ . Then, considering a homogeneous and isotropic universe background, the power spectrum  $\mathcal{P}_\zeta$  and the non-linearity parameter  $f_{\text{NL}}$  at the CMB scale in this model can be written as [37]

$$\mathcal{P}_\zeta = (\mathcal{N}_\phi^2 + \mathcal{N}_\sigma^2) \left( \frac{H_*}{2\pi} \right)^2, \quad (5.1)$$

$$f_{\text{NL}} = \frac{5}{6} \frac{\mathcal{N}_\phi^2 \mathcal{N}_{\phi\phi} + \mathcal{N}_\sigma^2 \mathcal{N}_{\sigma\sigma} + 2\mathcal{N}_\sigma \mathcal{N}_\phi \mathcal{N}_{\phi\sigma}}{(\mathcal{N}_\phi^2 + \mathcal{N}_\sigma^2)^2}, \quad (5.2)$$

at the leading order in terms of the field fluctuations. Here the subscripts  $\phi$  and  $\sigma$  denote partial derivatives with respect to the fields, i.e.  $\mathcal{N}_\phi \equiv \partial\mathcal{N}/\partial\phi_*$ ,  $\mathcal{N}_\sigma \equiv \partial\mathcal{N}/\partial\sigma_*$ , etc.

Given that the end of inflation is independent of  $\phi_*$  (so that quantities such as the energy density of the universe and the inflaton field value at the end of inflation are independent of  $\phi_*$ ), one can find that

$$\mathcal{N}_\phi = -\frac{H_*}{\dot{\phi}_*}, \quad (5.3)$$

where we have assumed that  $H$  and  $\dot{\phi}$  during inflation are determined merely by  $\phi$  (e.g., as in slow-roll inflation). Here we should remark that there are actually further contributions to  $\mathcal{N}_\phi$  since fluctuations in the duration of inflation due to  $\delta\phi$  lead to curvaton field fluctuations in the post-inflationary era, which can be seen as

$$\frac{\partial\sigma_{\text{osc}}}{\partial\phi_*} = (1 - X(\sigma_{\text{osc}}))^{-1} \frac{V'(\sigma_{\text{osc}})}{3H_*\dot{\phi}_*}. \quad (5.4)$$

This can be derived in a similar fashion as (2.23), considering a curvaton potential  $V(\sigma)$  that is a function only of  $\sigma$ . In this sense, the inflaton can further produce density perturbations after inflation by fluctuating the curvaton. Moreover, we note that such effect sources  $\mathcal{N}_{\phi\sigma}$ , which otherwise vanishes since the inflaton and curvaton only affect the e-folding numbers during and after inflation, respectively. However, in this section, we ignore effects due to (5.4)



since we would like to show that  $f_{\text{NL}}$  can become largely scale-dependent simply by having multiple sources (even in the absence of the cross term  $\mathcal{N}_{\phi\sigma}$ ), and also because their effects are negligible for the case of a quadratic curvaton and a slow-rolling inflaton which we will study later in this section<sup>#17</sup>.

For convenience, we introduce a parameter which represents the fraction of the curvaton contribution to the total power spectrum:

$$q \equiv \frac{\mathcal{N}_\sigma^2}{\mathcal{N}_\phi^2 + \mathcal{N}_\sigma^2}. \quad (5.5)$$

This quantity satisfies  $0 \leq q \leq 1$  by definition. Then using this quantity, the power spectrum and the non-linearity parameter  $f_{\text{NL}}$  can be rewritten as

$$\mathcal{P}_\zeta = \frac{1}{q} \mathcal{N}_\sigma^2 \left( \frac{H_*}{2\pi} \right)^2, \quad (5.6)$$

$$f_{\text{NL}} = \frac{5}{6} \left[ (1-q)^2 \frac{\mathcal{N}_{\phi\phi}}{\mathcal{N}_\phi^2} + q^2 \frac{\mathcal{N}_{\sigma\sigma}}{\mathcal{N}_\sigma^2} \right]. \quad (5.7)$$

Now let us write down the expressions in terms of the effective potentials. We assume that the inflaton and the curvaton are decoupled from each other so that the total potential can be divided into the inflaton potential  $U(\phi)$  which drives inflation as well as determines the inflaton dynamics, and the curvaton potential  $V(\sigma)$  which governs the curvaton dynamics. Both potentials are considered to have no explicit dependence on time. Furthermore, for the inflaton, we assume a slow-roll inflation, i.e.

$$3H\dot{\phi} = -U', \quad 3H^2 M_p^2 = U, \quad (5.8)$$

where a prime on  $U$  denotes differentiation with respect to  $\phi$ . These approximations give

$$\mathcal{N}_\phi = \frac{U}{M_p^2 U'} \Big|_*, \quad \mathcal{N}_{\phi\phi} = \frac{1}{M_p^2} \left( 1 - \frac{UU''}{U'^2} \right) \Big|_*. \quad (5.9)$$

Introducing the slow-roll parameters

$$\epsilon \equiv \frac{M_p^2}{2} \left( \frac{U'}{U} \right)^2, \quad \eta \equiv M_p^2 \frac{U''}{U}, \quad (5.10)$$

one arrives at

$$\frac{\mathcal{N}_{\phi\phi}}{\mathcal{N}_\phi^2} = 2\epsilon_* - \eta_*. \quad (5.11)$$

---

<sup>#17</sup> To be precise, for the mixed case of a quadratic curvaton (with mass  $m$ ) and a slow-rolling inflaton, effects from (5.4) on the power spectrum  $\mathcal{P}_\zeta$  are suppressed by a factor  $m^2/H_*^2$  compared to the contribution (5.3). As for  $f_{\text{NL}}$ , unless  $\hat{r}$  takes a specific value  $\hat{r} \approx 1.85$  which vanishes  $\mathcal{N}_{\sigma\sigma}/\mathcal{N}_\sigma^2$ , contributions from (5.4) on  $f_{\text{NL}}$  are either sufficiently smaller than unity, or subleading compared to other terms.

The curvaton is also assumed to slow-roll during inflation, i.e.  $3H\dot{\sigma} = -V'$ , where a prime here for  $V$  denotes a derivative in terms of  $\sigma$ . For the  $\delta\mathcal{N}$  from the curvaton we adopt the formulae used in Section 2:  $\mathcal{N}_\sigma$  is shown in (2.6), and  $\mathcal{N}_{\sigma\sigma}$  can be read off from (2.14).

Then, at the leading order in terms of the slow-roll parameters  $\epsilon_*$  and  $\eta_*$ , we obtain expressions for the spectral index  $n_s - 1$ , its running  $\alpha$ , and the product  $n_{f_{\text{NL}}}f_{\text{NL}}$  as follows:

$$n_s - 1 \simeq (1 - q)(-6\epsilon_* + 2\eta_*) + q \left( -2\epsilon_* + 2\frac{V''(\sigma_*)}{3H_*^2} \right), \quad (5.12)$$

$$\begin{aligned} \alpha \simeq & (1 - q) \left( -24\epsilon_*^2 + 16\epsilon_*\eta_* - 2\xi_* \right) \\ & + 4q(1 - q) \left( 2\epsilon_* - \eta_* + \frac{V''(\sigma_*)}{3H_*^2} \right)^2 \\ & + q \left( -8\epsilon_*^2 + 4\epsilon_*\eta_* + 4\epsilon_*\frac{V''(\sigma_*)}{3H_*^2} - 2\frac{V'(\sigma_*)V'''(\sigma_*)}{9H_*^4} \right), \end{aligned} \quad (5.13)$$

$$\begin{aligned} n_{f_{\text{NL}}}f_{\text{NL}} \simeq & \frac{5}{6} \left[ (1 - q)^2(8\epsilon_*^2 - 6\epsilon_*\eta_* + \xi_*) \right. \\ & + 4q(1 - q) \left( 2\epsilon_* - \eta_* + \frac{V''(\sigma_*)}{3H_*^2} \right) \left( (1 - q)(-2\epsilon_* + \eta_*) + q\frac{\mathcal{N}_{\sigma\sigma}}{\mathcal{N}_\sigma^2} \right) \\ & \left. + \frac{q^2}{\mathcal{N}_\sigma} \frac{V'''(\sigma_*)}{3H_*^2} \right], \end{aligned} \quad (5.14)$$

where we have further introduced another slow-roll parameter for the inflaton:

$$\xi \equiv M_p^4 \frac{U'U'''}{U^2}. \quad (5.15)$$

Let us stress that upon obtaining the above results, we have made use of the slow-roll approximations for  $\phi$  and  $\sigma$ , and further used the analytic formulae for  $\mathcal{N}_\sigma$  and  $\mathcal{N}_{\sigma\sigma}$  which also relies on some approximations (including the sudden decay) as discussed in Section 2. It should be noted that errors contained in the approximations can accumulate, especially as one goes to higher order derivatives.

The running of  $f_{\text{NL}}$  receives additional contributions in the mixed case from the second line of (5.14), which is absent for a pure curvaton or inflaton case. In particular, large  $f_{\text{NL}}$  and  $n_{f_{\text{NL}}}$  can be obtained when the curvaton mainly contributes to the (running) non-Gaussianity, while the inflaton mainly generates the linear order perturbations. In fact, the running  $\alpha$  also has the contribution specific to the mixed model such as the second line of (5.13). However, it is suppressed as  $(\mathcal{O}(\epsilon_*, \eta_*, \eta_\sigma))^2$  with  $\eta_\sigma = V''/(3H_*^2)$  corresponding to a slow-roll parameter for  $\sigma$ , hence  $\alpha$  is small in this model.

To see to what extent the running of non-Gaussianity can be large in this kind of model, as an example, let us consider a quadratic curvaton  $V(\sigma) = \frac{1}{2}m^2\sigma^2$  for which  $n_{f_{\text{NL}}}$  vanishes for the curvaton-only case, i.e.  $q = 1$ . (Note that for quadratic curvatons,  $f_{\text{NL}}$  and  $n_{f_{\text{NL}}}$  are

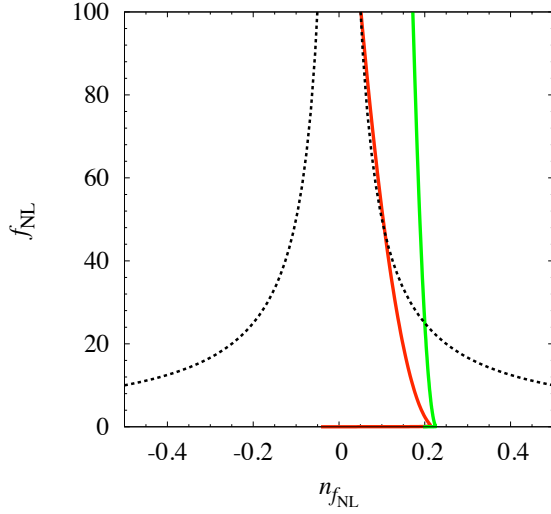


Figure 21: Contours for  $\hat{r} = 10^{-2}$  (red line) and  $10^{-3}$  (green line) with  $q$  being varied in the  $n_{f_{\text{NL}}}$ - $f_{\text{NL}}$  plane. Here we assume that  $m^2/(3H_*^2) = 0.05$ . The slow-roll parameters for the inflaton sector are taken as  $\epsilon_* = 0.016$ ,  $\eta_* = 0.025$ , and  $\xi_* = 0.0004$ . The expected observational sensitivity of Planck is also shown (black dashed).

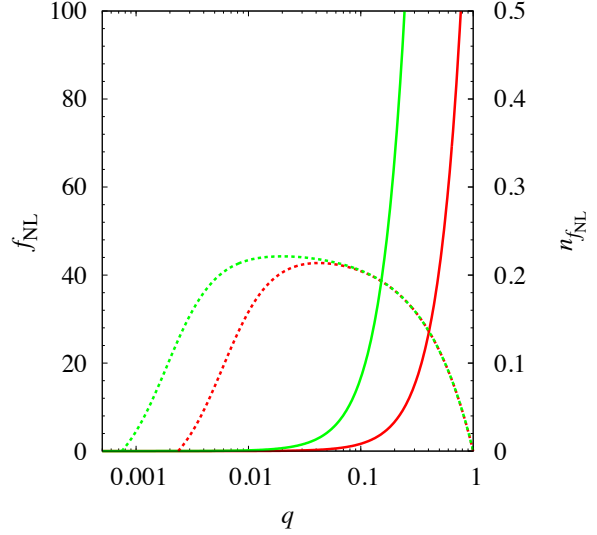


Figure 22: The same cases as Figure 21 are shown as a function of  $q$ .  $f_{\text{NL}}$  is plotted for  $\hat{r} = 10^{-2}$  (red) and  $10^{-3}$  (green).  $n_{f_{\text{NL}}}$  is for  $\hat{r} = 10^{-2}$  (red dashed) and  $\hat{r} = 10^{-3}$  (green dashed). Notice that the value of  $n_{f_{\text{NL}}}$  becomes insensitive to  $\hat{r}$  as  $q$  approaches to unity.

independent of  $\sigma_*$  and  $\sigma_{\text{osc}}$ .) By doing this, we can see  $n_{f_{\text{NL}}}$  generated from the multi-source nature of this scenario.

Given that  $\epsilon_*$ ,  $|\eta_*|$ ,  $|\xi_*|$ ,  $m^2/H_*^2 \ll 1$ , then one can check that  $|f_{\text{NL}}| \gg 1$  along with  $|n_{f_{\text{NL}}} f_{\text{NL}}| \gtrsim 1$  are realized if and only if

$$\hat{r} \lesssim q^2(1-q) \left| 2\epsilon_* - \eta_* + \frac{m^2}{3H_*^2} \right| \quad (5.16)$$

is satisfied. In such a case,  $f_{\text{NL}}$  and its running are approximated by

$$f_{\text{NL}} \simeq \frac{5q^2}{3\hat{r}}, \quad n_{f_{\text{NL}}} \simeq 4(1-q) \left( 2\epsilon_* - \eta_* + \frac{m^2}{3H_*^2} \right). \quad (5.17)$$

In Figure 21, plots in the  $n_{f_{\text{NL}}}$ - $f_{\text{NL}}$  plane are shown for cases with  $\hat{r} = 10^{-2}$  and  $10^{-3}$  with  $q$  being varied. For the curvaton mass, we assume  $m^2/(3H_*^2) = 0.05$ . The slow-roll parameters for the inflaton sector are taken as  $\epsilon_* = 0.016$ ,  $\eta_* = 0.025$ , and  $\xi_* = 0.0004$ , which correspond to the values for  $\phi^4$  chaotic inflation model with  $\mathcal{N}_* = 60$ . Since non-Gaussianity mainly comes from the curvaton sector,  $f_{\text{NL}}$  becomes larger as  $q$  approaches unity as read off

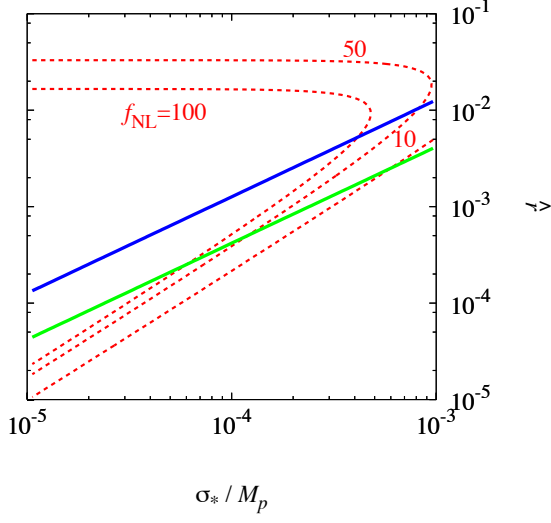


Figure 23: Contours of  $f_{\text{NL}}$  and  $n_{f_{\text{NL}}}$  in  $\sigma_*/M_p$ - $\hat{r}$  plane. Here we show the contours of  $n_{f_{\text{NL}}} = 0.2$  (green) and  $0.1$  (blue). The values of  $f_{\text{NL}}$  are shown in the figure. Other parameters are assumed as  $m^2/(3H_*^2) = 0.05$ ,  $\epsilon_* = 0.016$ ,  $\eta_* = 0.025$ , and  $\xi_* = 0.0004$ .

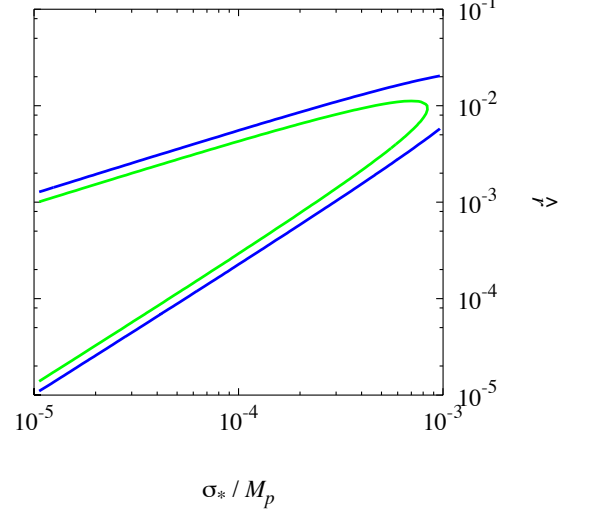


Figure 24: Shown are contours of  $n_{f_{\text{NL}}} f_{\text{NL}} = 5$  (green) and  $2.5$  (blue), which correspond to the detection limit values for Planck and CMBPol, respectively. Other parameters are taken as the same as in Figure 23.

from (5.17). But on the other hand,  $n_{f_{\text{NL}}}$  becomes small in this limit because the running of the non-Gaussianity arises due to the multi-source nature of the model and the case with  $q \rightarrow 1$  corresponds to the single-source limit.

Regarding the scale dependence of  $f_{\text{NL}}$ ,  $n_{f_{\text{NL}}}$  takes its maximum value at intermediate range of  $q$  since one has to have non-zero value of  $q(1-q)$  to have sizable  $n_{f_{\text{NL}}}$  in this kind of a mixed model. It should be noted here that although the value of  $f_{\text{NL}}$  becomes very small as  $q$  goes to 0, however, if we assume a very small value  $\hat{r}$  by choosing some appropriate parameters for the curvaton sector, the smallness of  $q$  is somewhat compensated and  $f_{\text{NL}}$  can be sizable. Thus for some values of  $q$ , both  $f_{\text{NL}}$  and  $n_{f_{\text{NL}}}$  can be large enough to be detected by Planck satellite as seen from Figure 21. To see how  $f_{\text{NL}}$  and  $n_{f_{\text{NL}}}$  depend on  $q$ , we also plot the values of these quantities as a function of  $q$  in Figure 22, from which we can clearly see how the size of  $q$  affects these quantities.

Since  $q$  is determined once we fix  $\epsilon_*$ ,  $\sigma_*$  and  $\hat{r}$ , we also show the prediction of the model in

the  $\sigma_*$ - $\hat{r}$  plane in Figure 23 where contours of  $f_{\text{NL}}$  and  $n_{f_{\text{NL}}}$  are shown. As already mentioned in the previous section, the detectability of  $n_{f_{\text{NL}}}$  rather depends on the product of  $n_{f_{\text{NL}}} f_{\text{NL}}$ , hence we further plot contours of this quantity in Figure 24. In the figure, the contours corresponding to the detection sensitivity limit for Planck and CMBPol are depicted. From the figure, we can see that, in some parameter region,  $n_{f_{\text{NL}}}$  can be detectable in near future observations.

## 6 Multi-curvaton

As a final example model related to the curvaton, we in this section consider the multi-curvaton scenario where multiple curvaton fields can be responsible for cosmic density perturbations. Models of this kind have been investigated in the literature [39, 40] and some explicit examples in particle physics have also been discussed [52]. In this section, we again neglect the contribution from the inflaton fluctuations to the total curvature perturbations. Although there may generally exist many curvaton fields, here we consider a two curvaton case.

As in the previous sections, first we write down the expressions for the spectral index  $n_s$ , the running  $\alpha$ , non-linearity parameter  $f_{\text{NL}}$ , and its running  $n_{f_{\text{NL}}}$ . In general, the curvature perturbations in the model can be written as, up to the second order of the field fluctuations,

$$\zeta = \mathcal{N}_a \delta a_* + \mathcal{N}_b \delta b_* + \frac{1}{2} (\mathcal{N}_{aa} (\delta a_*)^2 + \mathcal{N}_{bb} (\delta b_*)^2 + 2\mathcal{N}_{ab} \delta a_* \delta b_*), \quad (6.1)$$

where  $\delta a_*$  and  $\delta b_*$  are fluctuations of the curvaton fields “ $a$ ” and “ $b$ ”, respectively, and  $\mathcal{N}_a = \partial \mathcal{N} / \partial a_*$  and so on. Throughout this section, we denote “ $a$ ” and “ $b$ ” curvatons as the ones that decay first and later, respectively.

The explicit forms of  $\mathcal{N}_a$ ,  $\mathcal{N}_b$ , etc., can be expressed in terms of the curvaton potentials by extending the discussions in Section 2 to the multiple curvaton case. However, since the explicit expressions are in general very complicated and we are interested in the scale-dependence which comes from the multi-source nature of this scenario, here we limit ourselves to the case where the curvaton potentials are quadratic, i.e.,

$$V(a, b) = \frac{1}{2} m_a^2 a^2 + \frac{1}{2} m_b^2 b^2. \quad (6.2)$$

We do not specify which of the masses  $m_a$  and  $m_b$  is larger. We further suppose that the curvatons start to oscillate after the inflaton decay, and that the energy density of the curvatons are negligibly tiny compared to the total energy of the universe until both curvatons start their oscillations. Then, one can find that  $\mathcal{N}_a$ ,  $\mathcal{N}_{aa}$ ,  $\dots$  are of the form

$$\mathcal{N}_a \propto \frac{1}{a_*}, \quad \mathcal{N}_{aa} \propto \frac{1}{a_*^2}, \quad \mathcal{N}_{ab} \propto \frac{1}{a_* b_*}, \quad (6.3)$$

(the same for replacing  $a$  with  $b$ ), where the constants of proportionality are given as functions of the ratios between the energy densities of  $a$ ,  $b$ , and radiation upon decays of  $a$  and  $b$  (the

full expressions of the coefficients up to the third order are given in [38], where the density perturbations are computed in a different approach from Section 2):

$$\hat{r}_{a1} \equiv \frac{\rho_a}{\rho_r} \Big|_{t=t_{a\text{dec}}}, \quad \hat{r}_{b1} \equiv \frac{\rho_b}{\rho_r} \Big|_{t=t_{a\text{dec}}}, \quad \hat{r}_{b2} \equiv \frac{\rho_b}{\rho_r} \Big|_{t=t_{b\text{dec}}}. \quad (6.4)$$

Here we have defined  $\hat{r}_{a1}$  and  $\hat{r}_{b2}$  similarly to  $\hat{r}$  defined in (2.8).  $\rho_a, \rho_b$  and  $\rho_r$  are energy densities of  $a$  curvaton,  $b$  curvaton and radiation, respectively, while  $t_{a\text{dec}}$  and  $t_{b\text{dec}}$  are the times at the decay of  $a$  and  $b$  curvatons. Notice that  $\hat{r}_{a1}$  and  $\hat{r}_{b2}$  are defined at different times, thus we also put the subscripts “1” and “2” in addition to “ $a$ ” and “ $b$ ” in the definitions. We also remark that the  $\rho_r$  in the denominators of  $\hat{r}_{a1}$  and  $\hat{r}_{b1}$  come from the inflaton decay, while  $\rho_r$  in  $\hat{r}_{b2}$  also includes the decay products from the  $a$  curvaton.

Since the proportionality factors in (6.3) are determined by the three ratios (6.4), the scale-dependence of the density perturbations are sourced through  $a_*$  and  $b_*$ . Hence the spectral index  $n_s$  and its running  $\alpha$  for the power spectrum are (assuming Gaussian field fluctuations in the sense explained below (2.13), with  $\mathcal{P}_{\delta a}(k) = \mathcal{P}_{\delta b}(k) = (H|_{k=aH}/2\pi)^2$  when  $k$  exits the horizon, and no correlations between  $\delta a$  and  $\delta b$ )

$$n_s - 1 \simeq 2 \frac{\dot{H}_*}{H_*^2} + 2K_a \eta_a + 2K_b \eta_b, \quad (6.5)$$

$$\alpha \simeq 2 \frac{\ddot{H}_*}{H_*^3} - 4 \frac{\dot{H}_*^2}{H_*^4} - 4 \frac{\dot{H}_*}{H_*^2} (K_a \eta_a + K_b \eta_b) + 4K_a K_b (\eta_a - \eta_b)^2, \quad (6.6)$$

where  $\eta_a$  and  $\eta_b$  are defined as

$$\eta_a \equiv \frac{m_a^2}{3H_*^2}, \quad \eta_b \equiv \frac{m_b^2}{3H_*^2}. \quad (6.7)$$

We have also introduced the parameters  $K_a$  and  $K_b$  representing the fractional contribution of the curvatons  $a$  and  $b$  to the total power spectrum:

$$K_a \equiv \frac{\mathcal{N}_a^2}{\mathcal{N}_a^2 + \mathcal{N}_b^2}, \quad K_b \equiv \frac{\mathcal{N}_b^2}{\mathcal{N}_a^2 + \mathcal{N}_b^2}, \quad (6.8)$$

which clearly satisfies  $K_a + K_b = 1$ .

Regarding the non-Gaussianity, the non-linearity parameter  $f_{\text{NL}}$  is generally given by

$$f_{\text{NL}} = \frac{5}{6} \left( K_a^2 \frac{\mathcal{N}_{aa}}{\mathcal{N}_a^2} + K_b^2 \frac{\mathcal{N}_{bb}}{\mathcal{N}_b^2} + 2K_a K_b \frac{\mathcal{N}_{ab}}{\mathcal{N}_a \mathcal{N}_b} \right), \quad (6.9)$$

and its running  $n_{f_{\text{NL}}}$  can be computed as

$$n_{f_{\text{NL}}} f_{\text{NL}} \simeq \frac{10}{3} K_a K_b (\eta_a - \eta_b) \left[ K_a \frac{\mathcal{N}_{aa}}{\mathcal{N}_a^2} - K_b \frac{\mathcal{N}_{bb}}{\mathcal{N}_b^2} - \frac{\mathcal{N}_{ab}}{\mathcal{N}_a \mathcal{N}_b} (K_a - K_b) \right]. \quad (6.10)$$

In the limit of either one of these curvatons being solely responsible for density fluctuations (i.e., in the limit of  $K_a(K_b) \rightarrow 1$  and  $K_b(K_a) \rightarrow 0$ ), the above formulae reduce to a single curvaton case. What is specific to this model is the terms with  $K_a K_b$  which disappear in a single curvaton scenario. In particular, when the masses of two curvatons are different (i.e.,  $\eta_a \neq \eta_b$ ), the running  $n_{f_{\text{NL}}}$  can be sizable, which has been pointed out in [29, 30]. In fact,  $\alpha$  also receives the contribution which originates from the mass difference of the curvatons. However, as seen from (6.6), such a term is suppressed with  $(\eta_a - \eta_b)^2$ , thus  $\alpha$  would be small in this model.

In fact, even if we assume a quadratic potential for the curvatons, general expressions for the coefficients such as  $\mathcal{N}_a, \mathcal{N}_{aa}$  and so on are still very complicated. Thus in the following we discuss some limiting cases where both curvatons are *subdominant* and *dominant* at the time of their decays, paying particular attention to the non-linearity parameter  $f_{\text{NL}}$  and its running  $n_{f_{\text{NL}}}$ .

## 6.1 Both curvaton subdominant at their decays

First we consider the case where the energy densities of both curvatons at their decays are subdominant, i.e.,

$$\hat{r}_{a1}, \hat{r}_{b2} \ll 1. \quad (6.11)$$

Since we adopt a purely quadratic potential for the curvatons, we can treat the curvatons as nonrelativistic fluids once they start to oscillate. By using the sudden decay approximation, one can show that the explicit forms of (6.3) in this case become [38]<sup>#18</sup>

$$N_a \simeq \frac{\hat{r}_{a1}}{2} \frac{1}{a_*}, \quad N_b \simeq \frac{\hat{r}_{b2}}{2} \frac{1}{b_*}, \quad N_{aa} \simeq \frac{\hat{r}_{a1}}{2} \frac{1}{a_*^2}, \quad N_{ab} \simeq -\frac{3\hat{r}_{a1}\hat{r}_{b2}}{4} \frac{1}{a_* b_*}, \quad N_{bb} \simeq \frac{\hat{r}_{b2}}{2} \frac{1}{b_*^2}, \quad (6.12)$$

which give  $n_s, \alpha, f_{\text{NL}}$ , and  $n_{f_{\text{NL}}}$  through the formulae given in (6.5)–(6.10). For convenience, we also introduce a parameter representing the ratio of the amplitude of the  $a$  and  $b$  curvatons:

$$\lambda \equiv \frac{b_*}{a_*}. \quad (6.13)$$

In Figure 25, we plot  $f_{\text{NL}}$  and  $n_{f_{\text{NL}}}$  as functions of  $\lambda$  for several parameter sets of  $(\hat{r}_{a1}, \hat{r}_{b1}, \hat{r}_{b2}, \eta_a, \eta_b)$ <sup>#19</sup>. Actually, these parameters are not independent, as will be discussed around (6.16). Here we take different values for  $\eta_a$  and  $\eta_b$ <sup>#20</sup>, which can give a sizable value

<sup>#18</sup>To be precise, here we are also assuming that the decays of the curvatons  $a$  and  $b$  are well separated along the expansion timeline.

<sup>#19</sup>For completeness, we also give the value of  $\hat{r}_{b1}$  used in plotting the figures since we use a full expression provided in [38] for the computations. However, we remark that its actual value is not important in this limit as can be noticed from (6.12) where an explicit dependence on  $\hat{r}_{b1}$  disappears.

<sup>#20</sup>As can be seen from (6.16), the parameters are not independent and  $\eta_b$  in the figure takes values much smaller than  $\eta_a$ . However, when  $\eta_b \ll \eta_a$  is satisfied, the explicit value of  $\eta_b$  is not important for obtaining  $f_{\text{NL}}$  and  $n_{f_{\text{NL}}}$ .

for  $n_{f_{\text{NL}}}$  as noted above. When fixing  $\hat{r}_{a1}$  and  $\hat{r}_{b2}$ , the fraction  $K_a$  increases together with  $\lambda$ . From (6.10), one can see that large values of  $n_{f_{\text{NL}}} f_{\text{NL}}$  would be obtained when  $K_a \sim K_b$  (corresponding to  $\lambda \sim \hat{r}_{b2}/\hat{r}_{a1} \sim \mathcal{O}(10^2)$  for the parameter sets assumed in Figure 25), otherwise the factor  $K_a K_b$  becomes very small. Furthermore, in the limit of both curvatons *subdominant* we are considering here, one has

$$\frac{\mathcal{N}_{aa}}{\mathcal{N}_a^2} \simeq \frac{2}{\hat{r}_{a1}}, \quad \frac{\mathcal{N}_{bb}}{\mathcal{N}_b^2} \simeq \frac{2}{\hat{r}_{b2}}, \quad \frac{\mathcal{N}_{ab}}{\mathcal{N}_a \mathcal{N}_b} \simeq -3. \quad (6.14)$$

Thus, when  $\hat{r}_{a1} \ll \hat{r}_{b2} \ll 1$  and  $K_a \sim K_b$  where both  $f_{\text{NL}}$  and  $n_{f_{\text{NL}}}$  can be large, the terms originating solely from  $a$  curvaton dominate in (6.9) and (6.10) (i.e.,  $K_a^2(\mathcal{N}_{aa}/\mathcal{N}_a^2)$  and  $K_a(\mathcal{N}_{aa}/\mathcal{N}_a^2)$  in the expressions of  $f_{\text{NL}}$  and  $n_{f_{\text{NL}}}$ , respectively). In this case, we can make a rough estimate of the values of  $f_{\text{NL}}$  and  $n_{f_{\text{NL}}}$  as

$$f_{\text{NL}} \simeq \frac{5}{3} K_a^2 \frac{1}{\hat{r}_{a1}}, \quad n_{f_{\text{NL}}} \simeq 4(1 - K_a)(\eta_a - \eta_b). \quad (6.15)$$

In fact, for the case with  $(\hat{r}_{a1}, \hat{r}_{b2}) \simeq (10^{-4}, 10^{-2})$ ,  $n_{f_{\text{NL}}}$  takes its maximum value at around  $K_a \sim 0.1$  ( $K_b \sim 0.9$ ). Since now we are assuming that  $\hat{r}_{a1} \ll 1$ , large  $f_{\text{NL}}$  is possible even with a relatively small value of  $K_a$ . Furthermore, although  $\eta_a$  gives a positive contribution to  $n_s$  (see (6.5)), small  $K_a$  together with  $\eta_b \simeq 0$  imply that the spectral index can be red-tilted when assuming a large field inflation model with  $\dot{H}_*/\dot{H}_*^2 \sim -\mathcal{O}(0.01)$ . Thus, in this model, we can have large  $f_{\text{NL}}$  and  $n_{f_{\text{NL}}}$  with red-tilted power spectrum for some parameter region.

As emphasized several times in the previous sections, the detectability of  $n_{f_{\text{NL}}}$  also depends on the size of  $f_{\text{NL}}$ , thus we also show a plot in the  $n_{f_{\text{NL}}}-f_{\text{NL}}$  plane in Figure 26. For reference, the detection limit lines for Planck  $|n_{f_{\text{NL}}} f_{\text{NL}}| = 5$  are also shown. In the figure, the value of  $\lambda$  is varied as in Figure 25. In some region, the predictions of the model for  $f_{\text{NL}}$  and  $n_{f_{\text{NL}}}$  are beyond the detectable sensitivity line, thus if  $n_{f_{\text{NL}}}$  is detected in future experiments, this model may also be a target of serious study.

We should also remark that in the case discussed above, a detectable level of  $n_{f_{\text{NL}}}$  can be obtained at the expense of fine-tuning of the parameters. Since here we are assuming that both curvatons begin their oscillations during the radiation dominated epoch after the inflaton reheating, the ratio of the energy densities between  $a$  and  $b$  curvatons at the time of  $a$  curvaton decay is given by (independently of whether  $m_a \leq m_b$ )

$$\frac{\hat{r}_{a1}}{\hat{r}_{b1}} = \frac{\rho_a}{\rho_b} \Big|_{t=t_{\text{adec}}} \sim \frac{1}{\lambda^2} \left( \frac{\eta_a}{\eta_b} \right)^{1/4}, \quad (6.16)$$

where for simplicity we have taken  $b_{\text{osc}}/a_{\text{osc}} \sim b_*/a_*$ . Therefore one sees that the parameter sets chosen in Figure 25 suppose the mass  $m_b$  to be extremely suppressed, much smaller than  $m_a$ . See also discussions in Footnote #20.



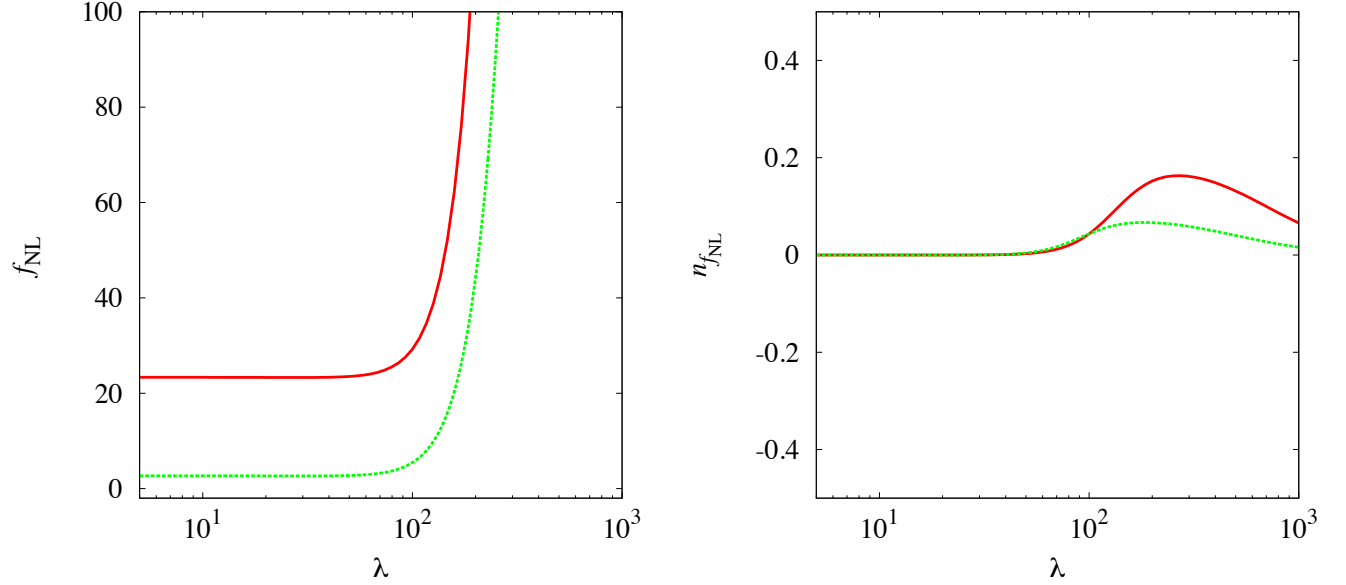


Figure 25: Plots of  $f_{\text{NL}}$  (left panel) and  $n_{f_{\text{NL}}}$  (right panel) as a function of  $\lambda$  for the cases with both curvatons being *subdominant* at their decays. Here we fix the parameters as  $(\hat{r}_{a1}, \hat{r}_{b1}, \hat{r}_{b2}, \eta_a) = (10^{-4}, 10^{-5}, 0.07, 0.05)$  (red) and  $(10^{-3}, 10^{-4}, 0.5, 0.02)$  (green), while  $\eta_b$  takes values much smaller than  $\eta_a$  (cf. Footnote #20).

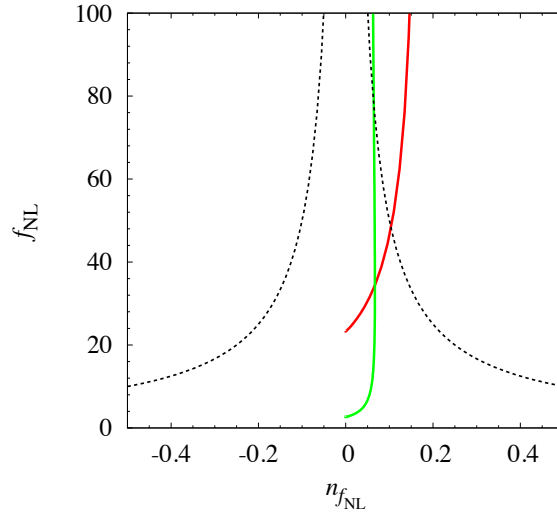


Figure 26: The same cases as Figure 25 are plotted in the  $f_{\text{NL}}-n_{f_{\text{NL}}}$  plane. The expected observational sensitivity of Planck is also shown (black dashed).

## 6.2 Both curvaton dominant at their decays

Now we consider the case where both curvatons are dominant at the time of their decays, i.e.,

$$\hat{r}_{a1}, \hat{r}_{b2} \gg 1, \quad \hat{r}_{a1} \gg \hat{r}_{b1}. \quad (6.17)$$

In this case, one obtains

$$N_a \simeq \frac{8}{9\hat{r}_{b2}} \frac{1}{a_*}, \quad N_b \simeq \frac{2}{3} \frac{1}{b_*}, \quad N_{aa} \simeq \frac{40}{27\hat{r}_{b2}} \frac{1}{a_*^2}, \quad N_{ab} \simeq -\frac{64}{27\hat{r}_{b2}} \frac{1}{a_* b_*}, \quad N_{bb} \simeq -\frac{2}{3} \frac{1}{b_*^2}. \quad (6.18)$$

It should be noted here that  $\zeta$  depends on  $\hat{r}_{b2}$  but not on  $\hat{r}_{a1}$  nor  $\hat{r}_{b1}$  at leading order as far as we assume the condition (6.17). Also one can easily see that

$$\frac{\mathcal{N}_{aa}}{\mathcal{N}_a^2} \simeq \frac{15\hat{r}_{b2}}{8}, \quad \frac{\mathcal{N}_{bb}}{\mathcal{N}_b^2} \simeq -\frac{3}{2}, \quad \frac{\mathcal{N}_{ab}}{\mathcal{N}_a \mathcal{N}_b} \simeq -4. \quad (6.19)$$

Hence, when the assumption of (6.17) holds and  $K_a \sim K_b$  where  $n_{f_{\text{NL}}}$  can be sizable,  $f_{\text{NL}}$  and  $n_{f_{\text{NL}}}$  are roughly estimated as

$$f_{\text{NL}} \simeq \frac{25}{16} K_a^2 \hat{r}_{b2}, \quad n_{f_{\text{NL}}} \simeq 4(1 - K_a)(\eta_a - \eta_b). \quad (6.20)$$

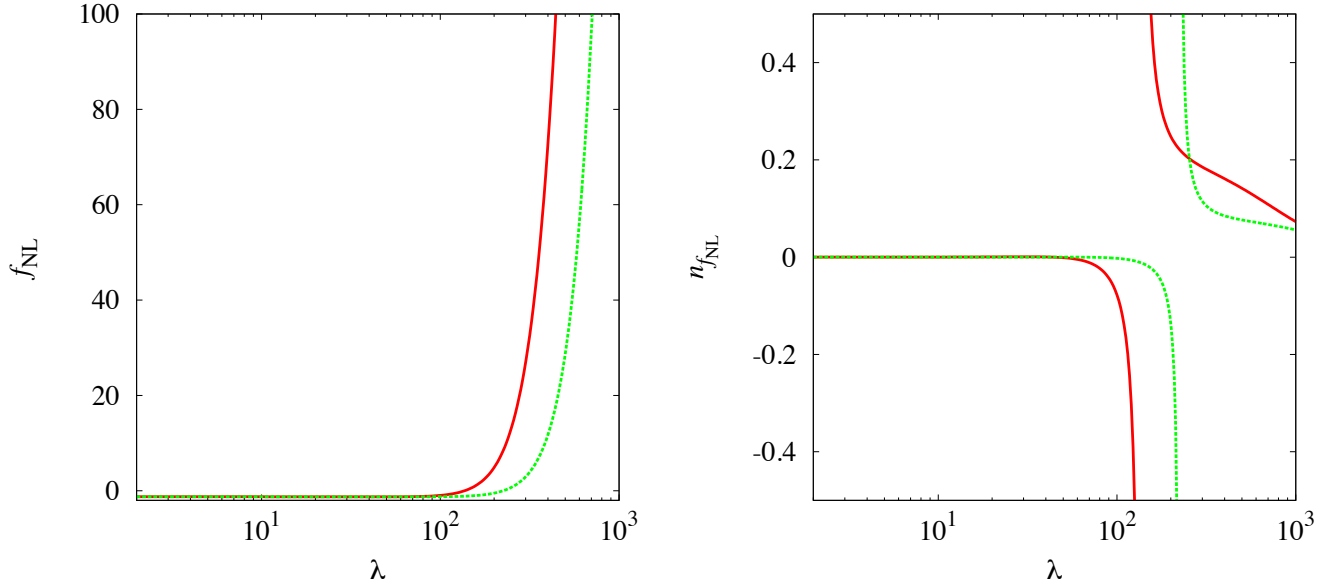


Figure 27: Plots of  $f_{\text{NL}}$  (left panel) and  $n_{f_{\text{NL}}}$  (right panel) as a function of  $\lambda$  for the cases with both curvatons being *dominant* at their decays. Here we fix the parameters as  $(\hat{r}_{a1}, \hat{r}_{b1}, \hat{r}_{b2}, \eta_a) = (10^3, 10^2, 10^3, 0.05)$  (red) and  $(10^3, 10^2, 2 \times 10^3, 0.02)$  (green), while  $\eta_b$  takes values much smaller than  $\eta_a$  (cf. Footnote #20).

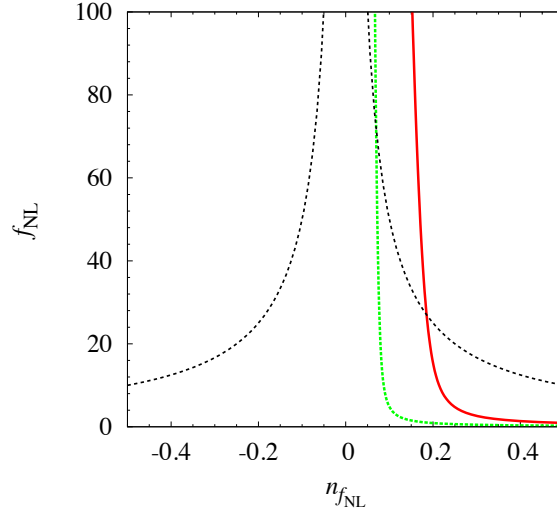


Figure 28: The same cases as Figure 27 are plotted in the  $f_{\text{NL}}-n_{f_{\text{NL}}}$  plane. The expected observational sensitivity of Planck is also shown (black dashed).

In Figure 27, we plot  $f_{\text{NL}}$  and  $n_{f_{\text{NL}}}$  as functions of  $\lambda$  for several parameter sets of  $(\hat{r}_{a1}, \hat{r}_{b1}, \hat{r}_{b2}, \eta_a, \eta_b)$ . As mentioned above, as long as we assume (6.17), the expressions for  $\mathcal{N}_a, \mathcal{N}_{aa}$  and so on are given as (6.18). Thus the assumption on the values of  $\hat{r}_{a1}$  and  $\hat{r}_{b1}$  have little effects on  $f_{\text{NL}}$  and  $n_{f_{\text{NL}}}$ . Under a fixed  $\hat{r}_{b2}$ , the fraction  $K_a$  increases along with  $\lambda$ . It should be noticed that  $f_{\text{NL}}$  becomes negative when  $\lambda$  is small, i.e.  $K_a \ll 1$ , due to the negative values of  $\mathcal{N}_{bb}/\mathcal{N}_b^2$ . However, as  $\lambda$  becomes larger ( $K_a$  is larger),  $f_{\text{NL}}$  crosses zero and increases to large positive values as seen from Figure 27. Hence  $n_{f_{\text{NL}}}$  blows up at around the region where  $f_{\text{NL}} \sim 0$  similarly to the case of the self-interacting curvaton. Further increasing  $\lambda$ , then  $K_a$  becomes comparable to  $K_b$  and (6.20) is satisfied. For even larger  $\lambda$ ,  $n_{f_{\text{NL}}}$  again becomes small. To see the detectability of  $n_{f_{\text{NL}}}$  in this case, we again show the plot in the  $n_{f_{\text{NL}}}-f_{\text{NL}}$  plane in Figure 28, from which we can clearly see that  $n_{f_{\text{NL}}}$  can be detectable in some parameter region as in the *subdominant* case discussed in the previous subsection. We remark that  $n_s$  can also be red-tilted at around the region where  $n_{f_{\text{NL}}}$  becomes large. In fact, with the parameter sets assumed in Figures 27 and 28, the contribution to the power spectrum from the  $a$  curvaton is somewhat small as  $K_a \sim \mathcal{O}(0.01)$  when  $n_{f_{\text{NL}}}$  blows up. There the positive contribution of  $K_a \eta_a$  in  $n_s$  becomes small, in which the spectral index can be almost given by  $n_s - 1 \simeq 2\dot{H}_*/H_*^2$  and be red-tilted for large field inflation models.

We also note that (6.16) requires the mass  $m_b$  to be highly suppressed in the above case, as in the previous subsection. Here, especially since the  $a$  curvaton is dominant at its decay, which means that  $\rho_a > \rho_b$ , the constraint (6.16) indicates  $\sqrt{m_a/m_b} > \lambda^2$ . As seen from Figure 27, the product of  $f_{\text{NL}} n_{f_{\text{NL}}}$  can be large when  $\lambda \sim \mathcal{O}(10^2)$ , which requires a large hierarchy between  $m_a$  and  $m_b$ .

## 7 Conclusions

In this paper we have investigated the scale-dependence of linear and second order density perturbations produced in the curvaton mechanism. In particular, we focused on the runnings such as  $\alpha$  and  $n_{f_{\text{NL}}}$ . Since models of the curvaton have several variants, we discussed the representative models: curvatons with non-quadratic potentials, and multiple source cases. For the later model, we discussed multi-curvaton and mixed curvaton and inflaton ones.

Non-quadratic curvaton potentials give scale-dependence to the non-Gaussianity, as well as to the spectral index of the linear perturbation spectrum. We have especially shown that the local-type  $f_{\text{NL}}$  produced from curvatons can strongly depend on the scale, even when the linear order perturbations are nearly scale-invariant. We analytically computed the running  $n_{f_{\text{NL}}} \equiv d \ln |f_{\text{NL}}| / d \ln k$  for curvatons with general energy potentials in (2.31), and obtained conditions (2.34) and (2.35) under which  $f_{\text{NL}}$  can be strongly scale-dependent.

The two conditions (2.34) and (2.35) can be satisfied respectively by curvaton potentials that flatten and steepen compared to a quadratic one. As an example of the former case, we looked into pseudo-Nambu-Goldstone curvatons with cosine-type potentials, for which it was shown that  $n_{f_{\text{NL}}}$  is directly related to the amplitude of  $\tilde{\alpha}$  and thus strictly constrained by current observational bounds on running spectral index, unless the inflationary mechanism realized a largely time-varying  $H$  such that cancelled out the contribution of  $\tilde{\alpha}$  to the running spectral index. For the latter case, we studied self-interacting curvatons in detail and saw that the steep potential wipes out the initial field fluctuations  $\delta\sigma_*$ , suppressing the resulting density perturbations. This lead to the production of a strongly scale-dependent  $f_{\text{NL}}$  even for a suppressed running spectral index, when  $\sigma_*$  was away from, but not too away from the potential minimum. Moreover, the scale-dependence of  $f_{\text{NL}}$  from self-interacting curvatons could be as large as to be detected by upcoming CMB experiments.

In Sections 5 and 6, we further discussed the mixed curvaton and inflaton, and multi-curvaton models. In these models, due to the multiple source nature, large values of  $n_{f_{\text{NL}}}$  can also arise in a different way from the conditions discussed for the curvaton only case. We have made quantitative discussion for the running and shown in what cases  $n_{f_{\text{NL}}}$  and  $f_{\text{NL}}$  can be both large enough to be detected in future cosmological observations.

The analytic methods used in this paper clarifies the intriguing behaviors of the density perturbations produced from non-quadratic and/or multiple curvatons, providing us with a systematic framework for studying the curvaton scenario in general. While for pseudo-Nambu-Goldstone curvatons a running  $f_{\text{NL}}$  was accompanied by a large  $\alpha$  and thus was constrained, the steep potential of self-interacting curvatons allowed strongly scale-dependent  $f_{\text{NL}}$ . We expect that in terms of the  $f_{\text{NL}}$  scale-dependence, these two examples respectively give typical behaviors of curvatons whose potentials flatten/steepen compared to a quadratic. Multiple source scenarios could also produce large  $n_{f_{\text{NL}}}$ . The systematic approach we presented will be helpful for probing the physics of curvatons when combined with upcoming data.

## Acknowledgements

T.K. would like to thank Neal Dalal, Teruaki Suyama, Fuminobu Takahashi, and Jun'ichi Yokoyama for helpful conversations. The work of T.T. is supported in part by JSPS Grant-in-Aid for Scientific Research No. 23740195 and also by Saga University Dean's Grant 2011 For Promising Young Researchers.

## A Density Perturbations from Curvatons with Non-Sinusoidal Oscillations

The analytic expressions in Section 2 can be generalized to include a period of non-sinusoidal oscillations, as was discussed in Appendix B of [28]. Here we suppose that the energy density of the oscillating curvaton initially redshifts as  $\rho_\sigma \propto a^{-n}$  with a constant  $n$ , then when its energy approaches a certain value  $\rho_{\sigma\text{sin}}$ , the curvaton suddenly switches to a sinusoidal oscillation and then redshifts as  $\rho_\sigma \propto a^{-3}$ . We take  $\rho_{\sigma\text{sin}}$  as a constant (i.e. independent of  $\sigma_*$ ), considering for e.g., self-interacting curvatons whose oscillations are determined by the curvaton field value. The curvaton energy density is assumed to be negligibly small until the inflaton decay or the onset of the curvaton oscillation, whichever is later.

Then the linear perturbation amplitude becomes

$$\mathcal{P}_\zeta = \left( \frac{\partial \mathcal{N}}{\partial \sigma_*} \frac{H_*}{2\pi} \right)^2, \quad (\text{A.1})$$

with

$$\frac{\partial \mathcal{N}}{\partial \sigma_*} = \frac{\hat{r}}{4 + 3\hat{r}} (1 - X(\sigma_{\text{osc}}))^{-1} \left\{ \frac{3}{n} \frac{V'(\sigma_{\text{osc}})}{V(\sigma_{\text{osc}})} - \frac{3X(\sigma_{\text{osc}})}{\sigma_{\text{osc}}} \right\} \frac{V'(\sigma_{\text{osc}})}{V'(\sigma_*)}, \quad (\text{A.2})$$

where  $X(\sigma_{\text{osc}})$  is defined in (2.9). The spectral index  $n_s$  and its running  $\alpha$  are the same as in (2.26) and (2.27), respectively. Furthermore, the non-linearity parameter is

$$\begin{aligned} f_{\text{NL}} = & \frac{40(1 + \hat{r})}{3\hat{r}(4 + 3\hat{r})} + \frac{5(4 + 3\hat{r})}{6\hat{r}} \left\{ \frac{3}{n} \frac{V'(\sigma_{\text{osc}})}{V(\sigma_{\text{osc}})} - \frac{3X(\sigma_{\text{osc}})}{\sigma_{\text{osc}}} \right\}^{-1} \left[ (1 - X(\sigma_{\text{osc}}))^{-1} X'(\sigma_{\text{osc}}) \right. \\ & + \left\{ \frac{3}{n} \frac{V'(\sigma_{\text{osc}})}{V(\sigma_{\text{osc}})} - \frac{3X(\sigma_{\text{osc}})}{\sigma_{\text{osc}}} \right\}^{-1} \left\{ \frac{3}{n} \frac{V''(\sigma_{\text{osc}})}{V(\sigma_{\text{osc}})} - \frac{3}{n} \frac{V'(\sigma_{\text{osc}})^2}{V(\sigma_{\text{osc}})^2} - \frac{3X'(\sigma_{\text{osc}})}{\sigma_{\text{osc}}} + \frac{3X(\sigma_{\text{osc}})}{\sigma_{\text{osc}}^2} \right\} \\ & \left. + \frac{V''(\sigma_{\text{osc}})}{V'(\sigma_{\text{osc}})} - (1 - X(\sigma_{\text{osc}})) \frac{V''(\sigma_*)}{V'(\sigma_{\text{osc}})} \right], \end{aligned} \quad (\text{A.3})$$

and its running takes the form

$$n_{f_{\text{NL}}} \simeq \frac{1}{f_{\text{NL}}} \frac{5(4 + 3\hat{r})}{18\hat{r}} \left\{ \frac{3}{n} \frac{V'(\sigma_{\text{osc}})}{V(\sigma_{\text{osc}})} - \frac{3X(\sigma_{\text{osc}})}{\sigma_{\text{osc}}} \right\}^{-1} (1 - X(\sigma_{\text{osc}})) \frac{V'(\sigma_*)}{V'(\sigma_{\text{osc}})} \frac{V'''(\sigma_*)}{H_*^2}. \quad (\text{A.4})$$

Of course, the above equations reproduce (2.6), (2.14), and (2.31) for purely sinusoidal oscillations, i.e.  $n = 3$ .

For example, for a self-interacting curvaton (4.1) with  $m = 4$ , then when  $\sigma_{\text{osc}}$  is larger than  $f$ , we need to use the expressions in this appendix with  $n = 4$ .

## References

- [1] K. Enqvist and M. S. Sloth, Nucl. Phys. B **626**, 395 (2002) [arXiv:hep-ph/0109214];
- [2] D. H. Lyth and D. Wands, Phys. Lett. B **524**, 5 (2002) [arXiv:hep-ph/0110002];
- [3] T. Moroi and T. Takahashi, Phys. Lett. B **522**, 215 (2001) [Erratum-ibid. B **539**, 303 (2002)] [arXiv:hep-ph/0110096].
- [4] E. Komatsu *et al.* [WMAP Collaboration], Astrophys. J. Suppl. **192**, 18 (2011) [arXiv:1001.4538 [astro-ph.CO]].
- [5] T. Moroi and H. Murayama, Phys. Lett. B **553**, 126 (2003) [hep-ph/0211019].
- [6] K. Enqvist, S. Kasuya and A. Mazumdar, Phys. Rev. Lett. **90**, 091302 (2003) [hep-ph/0211147].
- [7] M. Postma, Phys. Rev. D **67**, 063518 (2003) [hep-ph/0212005].
- [8] J. McDonald, Phys. Rev. D **68**, 043505 (2003) [hep-ph/0302222].
- [9] K. Enqvist, A. Jokinen, S. Kasuya and A. Mazumdar, Phys. Rev. D **68**, 103507 (2003) [hep-ph/0303165].
- [10] S. Kasuya, M. Kawasaki and F. Takahashi, Phys. Lett. B **578**, 259 (2004) [hep-ph/0305134].
- [11] K. Hamaguchi, M. Kawasaki, T. Moroi and F. Takahashi, Phys. Rev. D **69**, 063504 (2004) [hep-ph/0308174].
- [12] J. McDonald, Phys. Rev. D **69**, 103511 (2004) [hep-ph/0310126].
- [13] K. Enqvist, S. Kasuya and A. Mazumdar, Phys. Rev. Lett. **93**, 061301 (2004) [hep-ph/0311224].
- [14] M. Ikegami and T. Moroi, Phys. Rev. D **70**, 083515 (2004) [hep-ph/0404253].
- [15] R. Allahverdi, K. Enqvist, A. Jokinen and A. Mazumdar, JCAP **0610**, 007 (2006) [hep-ph/0603255].
- [16] T. Kobayashi and S. Mukohyama, JCAP **0907**, 032 (2009) [arXiv:0905.2835 [hep-th]].

- [17] C. P. Burgess, M. Cicoli, M. Gomez-Reino, F. Quevedo, G. Tasinato and I. Zavala, JHEP **1008**, 045 (2010) [arXiv:1005.4840 [hep-th]].
- [18] K. Enqvist and S. Nurmi, JCAP **0510**, 013 (2005) [astro-ph/0508573].
- [19] K. Enqvist and T. Takahashi, JCAP **0809**, 012 (2008) [arXiv:0807.3069 [astro-ph]].
- [20] Q. G. Huang, JCAP **0811**, 005 (2008) [arXiv:0808.1793 [hep-th]].
- [21] K. Enqvist, S. Nurmi, G. Rigopoulos, O. Taanila and T. Takahashi, JCAP **0911**, 003 (2009) [arXiv:0906.3126 [astro-ph.CO]].
- [22] K. Enqvist and T. Takahashi, JCAP **0912**, 001 (2009) [arXiv:0909.5362 [astro-ph.CO]].
- [23] K. Enqvist, S. Nurmi, O. Taanila and T. Takahashi, JCAP **1004**, 009 (2010) [arXiv:0912.4657 [astro-ph.CO]].
- [24] J. Fonseca and D. Wands, Phys. Rev. D **83**, 064025 (2011) [arXiv:1101.1254 [astro-ph.CO]].
- [25] K. Dimopoulos, D. H. Lyth, A. Notari and A. Riotto, JHEP **0307**, 053 (2003) [hep-ph/0304050].
- [26] M. Kawasaki, K. Nakayama and F. Takahashi, JCAP **0901**, 026 (2009) [arXiv:0810.1585 [hep-ph]].
- [27] P. Chingangbam and Q. G. Huang, JCAP **0904**, 031 (2009) [arXiv:0902.2619 [astro-ph.CO]].
- [28] M. Kawasaki, T. Kobayashi and F. Takahashi, Phys. Rev. D **84**, 123506 (2011) [arXiv:1107.6011 [astro-ph.CO]].
- [29] C. T. Byrnes, S. Nurmi, G. Tasinato and D. Wands, JCAP **1002**, 034 (2010) [arXiv:0911.2780 [astro-ph.CO]].
- [30] C. T. Byrnes, M. Gerstenlauer, S. Nurmi, G. Tasinato and D. Wands, JCAP **1010**, 004 (2010) [arXiv:1007.4277 [astro-ph.CO]].
- [31] C. T. Byrnes, K. Enqvist and T. Takahashi, JCAP **1009**, 026 (2010) [arXiv:1007.5148 [astro-ph.CO]].
- [32] Q. -G. Huang, JCAP **1011**, 026 (2010) [Erratum-ibid. **1102**, E01 (2011)] [arXiv:1008.2641 [astro-ph.CO]].
- [33] C. T. Byrnes, K. Enqvist, S. Nurmi and T. Takahashi, JCAP **1111**, 011 (2011) [arXiv:1108.2708 [astro-ph.CO]].

- [34] D. Langlois and F. Vernizzi, Phys. Rev. D **70**, 063522 (2004) [arXiv:astro-ph/0403258];
- [35] T. Moroi, T. Takahashi and Y. Toyoda, Phys. Rev. D **72**, 023502 (2005) [arXiv:hep-ph/0501007];
- [36] T. Moroi and T. Takahashi, Phys. Rev. D **72**, 023505 (2005) [arXiv:astro-ph/0505339];
- [37] K. Ichikawa, T. Suyama, T. Takahashi and M. Yamaguchi, Phys. Rev. D **78**, 023513 (2008) [arXiv:0802.4138 [astro-ph]].
- [38] T. Suyama, T. Takahashi, M. Yamaguchi and S. Yokoyama, JCAP **1012**, 030 (2010) [arXiv:1009.1979 [astro-ph.CO]].
- [39] K. -Y. Choi and J. -O. Gong, JCAP **0706**, 007 (2007) [arXiv:0704.2939 [astro-ph]].
- [40] H. Assadullahi, J. Valiviita and D. Wands, Phys. Rev. D **76**, 103003 (2007) [arXiv:0708.0223 [hep-ph]].
- [41] M. LoVerde, A. Miller, S. Shandera and L. Verde, JCAP **0804**, 014 (2008) [arXiv:0711.4126 [astro-ph]].
- [42] E. Sefusatti, M. Liguori, A. P. S. Yadav, M. G. Jackson and E. Pajer, JCAP **0912**, 022 (2009) [arXiv:0906.0232 [astro-ph.CO]].
- [43] A. Becker, D. Huterer and K. Kadota, JCAP **1101**, 006 (2011) [arXiv:1009.4189 [astro-ph.CO]].
- [44] S. Shandera, N. Dalal and D. Huterer, JCAP **1103**, 017 (2011) [arXiv:1010.3722 [astro-ph.CO]].
- [45] A. A. Starobinsky, JETP Lett. **42**, 152 (1985) [Pisma Zh. Eksp. Teor. Fiz. **42**, 124 (1985)].
- [46] M. Sasaki and E. D. Stewart, Prog. Theor. Phys. **95**, 71 (1996) [astro-ph/9507001].
- [47] D. Wands, K. A. Malik, D. H. Lyth and A. R. Liddle, Phys. Rev. D **62**, 043527 (2000) [astro-ph/0003278].
- [48] D. H. Lyth, K. A. Malik and M. Sasaki, JCAP **0505**, 004 (2005) [astro-ph/0411220].
- [49] E. Komatsu and D. N. Spergel, Phys. Rev. D **63**, 063002 (2001) [astro-ph/0005036].
- [50] [Planck Collaboration], astro-ph/0604069.
- [51] D. Baumann *et al.* [CMBPol Study Team Collaboration], AIP Conf. Proc. **1141**, 10 (2009) [arXiv:0811.3919 [astro-ph]].
- [52] L. -Y. Lee, C. -M. Lin and C. -S. Chen, arXiv:1105.2388 [hep-ph].